On the Strong Discontinuity Approach in Finite Deformation Settings

Theoretical Aspects and Numerical Simulation

J. Oliver
A. Huespe
D. Pulido
E. Samaniego

Monograph CIMNE Nº-62, October 2001

On the Strong Discontinuity Approach in Finite Deformation Settings

Theoretical Aspects and Numerical Simulation

J. Oliver
A.Huespe
D. Pulido
E. Samaniego

Monograph CIMNE Nº-62, October 2001

International Center for Numerical Methods in Engineering
Gran Capitán s/n, 08034 Barcelona, Spain

INTERNATIONAL CENTER FOR NUMERICAL METHODS IN ENGINEERING
Edificio C1, Campus Norte UPC
Gran Capitán s/n
08034 Barcelona, Spain

Primera edición October 2001

ON THE STRONG DISCONTINUITY APPROACH IN FINITE DEFORMATION SETTINGS
THEORETICAL ASPECTS AND NUMERICAL SIMULATION

Monografía CIMNE M62

ISBN: 84-89925-89-5

Depósito legal: B-48205-2001

Developers:
Ramón Ribó (ramsan@cimne.upc.es)
Miguel A. de Riera Pasenau (Miguel@cimne.upc.es)
Enrique Escolano (escolano@cimne.upc.es)

For further information please contact:
International Center for numerical Methods in Engineering
Edificio C1, Campus Norte UPC
Gran Capitán s/n, 08034 Barcelona, Spain
http://gid.cimne.upc.es

CN $Revisión: 1.73 $ July 2000

Depósito legal: B-35598-98
ISBN Reference Manual: 84-89925-83-6
ISBN Obra Completa: 84-89925-84-4

CONTENTS

PART 1

PART 2

On the strong discontinuity approach in finite deformation settings. Part 1: Theoretical aspects

Abstract

Taking the strong discontinuity approach as a framework for modeling displacement discontinuities and strain localization phenomena, this Part 1 extends previous results of the authors, for infinitesimal strain settings, to finite deformation scenarios.

By means of the strong discontinuity analysis, and for both damage and elastoplasticity continuum (stress-strain) constitutive models, projected discrete (tractions-displacement jumps) constitutive models are derived, together with the strong discontinuity conditions that restrict the stress states at the discontinuous regime. Also a variable bandwidth model, to automatically induce those strong discontinuity conditions, and a discontinuous bifurcation procedure, to determine the initiation and propagation of the discontinuity, are briefly sketched. Numerical simulation issues are tackled in Part 2 of the work.

keywords: Strong discontinuities, localization, fracture, damage, elastoplasticity, finite strains.

1 INTRODUCTION

Modelling the onset and development of material discontinuities (fractures, cracks, slip lines etc.) has been the object of intense research in solid mechanics during the last decades. Besides the classical nonlinear fracture mechanics approaches [24], one common way of modelling displacement discontinuities,

from the continuum mechanics point of view, has been the simulation of the strain localization phenomenon by using material models equipped with strain-softening. This can be justified not only from the physical point of view, since this mode of deformation can be observed either in ductile materials (see e.g. [32] and reference therein, [15]) or in quasibrittle materials (e.g. [33]), but also from the kinematic point of view, since strain localization induces relative displacements at both side of the localization band that can be interpreted as the displacement jumps. However, it is nowadays well known that classical continuum inviscid dissipative models featuring strain softening lead to ill-posed boundary value problems. This becomes particularly evident in numerical simulation contexts since the obtained finite element results exhibit strong mesh dependence and no convergence with mesh refinement.

Different remedies for this behavior have been presented in the literature. Basically, they are based on the modification of the classical inviscid constitutive response, by adding, to the stress-strain constitutive equation, higher-order deformation gradients, non-local dependence or rate dependence ([5]).

In recent years, a second group of procedures that resort to the *strong discontinuity* concept have been developed. They advocate the introduction of the *strong discontinuity kinematics*, i.e., the modification of the standard continuum kinematical descriptions to take into account the appearance of discontinuous displacement fields through material interfaces in the solid [29], [17], [2], [12], [11], [25]. A common issue associated to these procedures is the finite element technology, which should enable to capture jumps in the displacement field. For such purposes, new families of *elements with embedded discontinuities* have been developed ([8], [13], [18], [10], [3])

Considering the aforementioned strong discontinuity kinematics has some interesting consequences. In fact, it turns out [20] that under such a kinematics the standard *continuum* (stress-strain) constitutive models induce *discrete* (traction-displacement jump) constitutive models on the interface of discontinuity[1]. Those discrete models can then be regarded as projections of the original constitutive model on that discontinuity interface, and inherit the basic features of the *parent* continuum model [22], [20]. However, they can be only induced when a particular stress state has been reached at the

[1]A crucial condition for this to happen is that the strong discontinuity kinematics is linked to the continuum constitutive model through a constitutive regularization of the hardening/softening parameter. This allows the model to return bounded tractions for input unbounded strains

interface, which is therefore restricted by the so called *strong discontinuity conditions* [20].

Consequently, and regarding the way that the different models make use of those induced discrete models, and the format in which they are introduced into the analysis, they can be classified into:

1. *Discrete approaches* [8], [13], [34], [25]: They introduce a discrete constitutive model at the interface that is completely independent from the continuum one. Their connection with the strong discontinuity kinematics is limited to numerical aspects, essentially to the use of finite elements with embedded discontinuities.

2. *Discrete-continuum approaches* [2], [9], [11], [1]:They make use of the continuum induced discrete constitutive equation introducing it into the problem in a *discrete format*: i.e. the discrete constitutive equation is analytically derived and then introduced, as a separation law, at the discontinuous interface regardless the fulfillment of the strong discontinuity conditions.

3. *Continuum approaches*:

   A full use of the connections between the continuum and the induced discrete constitutive models is made. As a matter of fact the latter is never explicitly introduced at the discontinuous interface, but it is implicitly imposed from the former as a consequence of the activation of the strong discontinuity kinematics once the strong discontinuity conditions are fulfilled. As a result, the whole analysis and simulation is kept in the *continuum format*.

This paper focuses on this last continuum approach that, from now on, will be termed the *Strong Discontinuity Approach* (SDA). Its analysis and implications for infinitesimal strains settings have been presented by the authors in the past [16], [17], [18], [21], [19], [22], [20], [23]. Here we extend those results to the finite deformation setting for isotropic damage and elastoplastic material models.

The remaining of this paper is organized as follows: section 2 introduces the strong discontinuity kinematics in the large strain context. Then, in section 3, a strong discontinuity analysis is done for two material constitutive models: an isotropic continuum damage model and a classical J_2 elastoplastic

model. For both, the induced discrete constitutive models and the strong discontinuity conditions are derived. Finally the conclusions of this part of the work are presented.

Some other topics, like those of finite elements with embedded discontinuities or the numerical applications of the proposed methodology are postponed to the second part of this work.

Other issues, which are deemed of marginal interest, can be found in two final Appendixes devoted to the constitutive tangent tensors, the bifurcation conditions, and the determination of the normal to the discontinuity surface as well as the incremental integration algorithms.

2 STRONG DISCONTINUITY KINEMATICS

Let $\Omega \in \mathbb{R}^3$ be a body undergoing a mechanical process which displays a displacement field that is discontinuous across material surface $\mathcal{S} \subset \Omega$ (see figure 1a) with a jump in the velocity field given by $[\![\dot{\mathbf{u}}]\!] = \dot{\mathbf{u}}(\mathbf{X}_{\mathcal{S}^+}) - \dot{\mathbf{u}}(\mathbf{X}_{\mathcal{S}^-})$. The velocity field is described by :

$$\dot{\mathbf{u}}(\mathbf{X},t) = \dot{\bar{\mathbf{u}}}(\mathbf{X},t) + \mathcal{H}_s[\![\dot{\mathbf{u}}]\!](\mathbf{X},t) \; ; \quad \mathcal{H}_s(\mathbf{X}) = \begin{cases} 0 & \forall\, \mathbf{X} \in \Omega^- \\ 1 & \forall\, \mathbf{X} \in \Omega^+ \end{cases} \tag{1}$$

$\dot{\bar{\mathbf{u}}}(\mathbf{X})$ and $[\![\dot{\mathbf{u}}]\!]$ being two continuous (smooth) fields, $\mathcal{H}_s$ the step function (Heaviside function) and Ω^-, Ω^+ each one of the body's disjunct parts of Ω obtained from its division by the surface $\mathcal{S}$.

This mode is characterized by a material velocity gradient $\dot{\mathbf{F}}$:

$$\dot{\mathbf{F}} = \dot{\mathbf{u}} \otimes \boldsymbol{\nabla} = \dot{\bar{\mathbf{F}}} + \delta_{\mathcal{S}}([\![\dot{\mathbf{u}}]\!] \otimes \mathbf{N}) \tag{2}$$

where $\dot{\bar{\mathbf{F}}}$ is a bounded (regular) term, $\delta_{\mathcal{S}}$ the Dirac delta function on $\mathcal{S}$, and $\mathbf{N}$ a material (fixed) unit vector orthogonal to $\mathcal{S}$. The deformation gradient $\mathbf{F}(\mathbf{X},t)$, at time t, comes from the integration of equation (2) along time:

$$\mathbf{F}(\mathbf{X},t) \; = \int_0^t \dot{\bar{\mathbf{F}}} dt + \int_{t_{SD}}^t \delta_{\mathcal{S}}([\![\dot{\mathbf{u}}]\!] \otimes \mathbf{N}) dt = \underbrace{\bar{\mathbf{F}}}_{regular} + \delta_{\mathcal{S}}\,(\boldsymbol{\beta} \otimes \mathbf{N}) \tag{3}$$

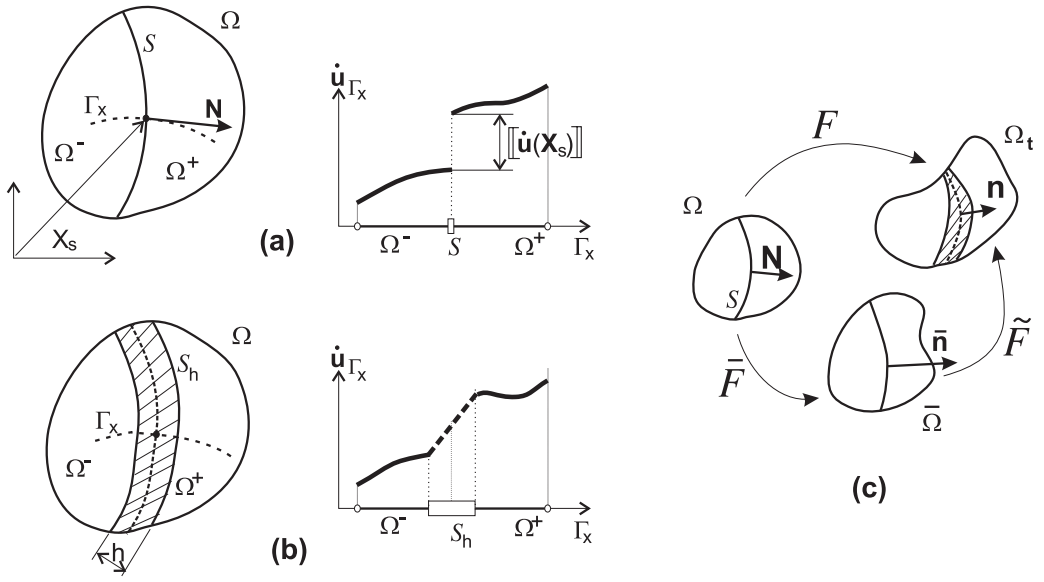

Figure 1: **(a)** strong discontinuity kinematic; **(b)** regularized kinematic; **(c)** multiplicative decomposition.

where t_{SD} stands for the onset time of the strong discontinuity mode and $\boldsymbol{\beta}$ is the incremental displacement jump between the current time, t, and t_{SD}:

$$\boldsymbol{\beta} = \mathbf{0} \; ; \qquad t < t_{SD} \tag{4a}$$

$$\boldsymbol{\beta} = [\![\mathbf{u}]\!]_t - [\![\mathbf{u}]\!]_{t_{SD}} \; ; \qquad t \geq t_{SD} \tag{4b}$$

Notice that in equation (3), the regular term $\bar{\mathbf{F}}$ remains bounded during all the process.

2.1 Multiplicative decomposition of the deformation gradient

For the subsequent analysis it is convenient to adopt, from equation (3), the multiplicative decomposition of the deformation gradient (see figure1c) proposed in [2]:

$$\mathbf{F} = \tilde{\mathbf{F}} \cdot \bar{\mathbf{F}} = [\mathbf{1} + \delta_{\mathcal{S}}(\boldsymbol{\beta} \otimes \bar{\mathbf{n}})] \cdot \bar{\mathbf{F}} \; ; \qquad \bar{\mathbf{n}} = \bar{\mathbf{F}}^{-T} \cdot \mathbf{N} \tag{5}$$

which introduces the concept of a *regular* intermediate configuration $\bar{\Omega}$, described by a $\mathbb{R}^3$ mapping whose gradient of deformation is regular and given by $\bar{\mathbf{F}}$. Notice that, in accordance with equation (5) $\bar{\mathbf{n}}$, the normal vector to the surface $\mathcal{S}$ convected by $\bar{\mathbf{F}} \neq \mathbf{1}$, is not a unit vector.

For the sake of simplicity in the subsequent mathematical analysis, we shall regularize the Dirac's delta function by defining a slice of the body $\mathcal{S}_h$ (see figure 1b), of finite thickness h, which contains the surface $\mathcal{S}$ ($\mathcal{S} \subset \mathcal{S}_h$). Then we consider the h-sequence of regular functions:

$$\delta^h_{\mathcal{S}} = \frac{\mu_{\mathcal{S}}}{h} \; ; \qquad \mu_{\mathcal{S}} = \left\{ \begin{array}{ll} 0 & \forall \, \mathbf{X} \notin \mathcal{S}_h \\ 1 & \forall \, \mathbf{X} \in \mathcal{S}_h \end{array} \right. \tag{6}$$

In the limit, as $h \to 0$, then $\delta_{\mathcal{S}_h} \to \delta_{\mathcal{S}}$.

Using this regularization, and after some algebraic manipulation, the following identities are obtained:

$$\dot{\mathbf{F}} = \dot{\bar{\mathbf{F}}} + \frac{\mu_{\mathcal{S}}}{h}(\dot{\boldsymbol{\beta}} \otimes \mathbf{N}) \tag{7}$$

$$\mathbf{F} = \bar{\mathbf{F}} + \tfrac{\mu_{\mathcal{S}}}{h}(\boldsymbol{\beta} \otimes \mathbf{N}) = \underbrace{\left(\mathbf{1} + \frac{\mu_{\mathcal{S}}}{h}\,(\,\boldsymbol{\beta} \otimes \bar{\mathbf{n}}\,)\right)}_{\tilde{\mathbf{F}}^h} \cdot \bar{\mathbf{F}} \;\; = \tilde{\mathbf{F}}^h \cdot \bar{\mathbf{F}} \tag{8}$$

$$\mathbf{F}^{-1} = \bar{\mathbf{F}}^{-1} \cdot (\tilde{\mathbf{F}}^h)^{-1} = \bar{\mathbf{F}}^{-1} \cdot \left(\mathbf{1} - \frac{\mu_{\mathcal{S}}}{h + \boldsymbol{\beta} \cdot \bar{\mathbf{n}}}(\boldsymbol{\beta} \otimes \bar{\mathbf{n}}) \right) \tag{9}$$

$$J = \det(\mathbf{F}) = \det(\bar{\mathbf{F}}) \left(1 + \frac{\mu_{\mathcal{S}}\, \boldsymbol{\beta} \cdot \bar{\mathbf{n}}}{h} \right) = \bar{J}\tilde{J}^h \tag{10}$$

$$\bar{J} = \det(\bar{\mathbf{F}}) \; ; \qquad \tilde{J}^h = \det(\bar{\mathbf{F}}^h) = \left(1 + \frac{\mu_{\mathcal{S}}\, \boldsymbol{\beta} \cdot \bar{\mathbf{n}}}{h} \right) \tag{11}$$

We also define $\mathbf{n}$ as the normal vector $\mathbf{N}$ convected by the total motion,

$$\mathbf{n} = \mathbf{F}^{-T} \cdot \mathbf{N} = \tilde{\mathbf{F}}^{h^{-T}} \cdot \bar{\mathbf{n}} = \frac{\bar{\mathbf{n}}}{\tilde{J}^h} \tag{12}$$

2.2 Rate of deformation tensors

Using the multiplicative decomposition (5) and equations (7) and (9), the regularized velocity gradient is obtained as follows[2]:

$$\mathbf{l} = \dot{\mathbf{F}} \cdot \mathbf{F}^{-1} = \bar{\mathbf{l}} + \tilde{\mathbf{l}} \tag{13}$$

where

$$\bar{\mathbf{l}} = \dot{\bar{\mathbf{F}}} \cdot \bar{\mathbf{F}}^{-1} \; ; \qquad \tilde{\mathbf{l}} = \mu_{\mathcal{S}} \frac{\bar{L}_{\bar{v}} \boldsymbol{\beta} \otimes \bar{\mathbf{n}}}{h + \boldsymbol{\beta} \cdot \bar{\mathbf{n}}} \tag{14}$$

and $\bar{L}_{\bar{v}} \boldsymbol{\beta} = \dot{\boldsymbol{\beta}} - \bar{\mathbf{l}} \boldsymbol{\beta}$ is the convected rate of $\boldsymbol{\beta}$ (the Lie derivative $\bar{L}_{\bar{v}}(\cdot)$ associated to the regular motion $\bar{\mathbf{F}}$) .

Then, the rate of deformation and spin tensors result :

$$\mathbf{d} = sym(\mathbf{l}) = \bar{\mathbf{d}} + \mu_{\mathcal{S}} \frac{(\bar{L}_{\bar{v}} \boldsymbol{\beta} \otimes \bar{\mathbf{n}})^{\mathrm{sym}}}{h + \boldsymbol{\beta} \cdot \bar{\mathbf{n}}} \tag{15}$$

$$\boldsymbol{\omega} = skew(\mathbf{l}) = \bar{\boldsymbol{\omega}} + \mu_{\mathcal{S}} \frac{(\bar{L}_{\bar{v}} \boldsymbol{\beta} \otimes \bar{\mathbf{n}})^{\mathrm{skw}}}{h + \boldsymbol{\beta} \cdot \bar{\mathbf{n}}} \tag{16}$$

where $\bar{\mathbf{d}}$ and $\bar{\boldsymbol{\omega}}$ are, respectively, the symmetric and skew-symmetric parts of $\bar{\mathbf{l}}$.

3 STRONG DISCONTINUITY ANALYSIS

In addition to the kinematics described in previous sections, the SDA lies on several assumptions and ingredients, some of them trying to match the physical aspects associated to the formation of a displacement discontinuity and some others of more mathematical nature. Those assumptions and their implications will be described in the following sections.

[2] From now on the superindex $(\cdot)^h$ to indicate the h-regularized version of entity $(\cdot)$ will be omitted.

3.1 Traction continuity: stress boundedness

The momentum balance principle for the quasistatic case, set in the classical weak form for the continuum domain Ω/S in terms of the nominal Piola-Kirchhoff stress tensor $\mathbf{P}(\mathbf{X}, \mathbf{t})$, reads:

$$\int_{\Omega\setminus S} \mathbf{P} : (\bar{\boldsymbol{\eta}} \otimes \nabla_{\mathbf{X}}) dV - \int_{\Omega} \bar{\mathbf{B}} \cdot \bar{\boldsymbol{\eta}} \; d\Omega - \int_{\Gamma_\sigma} \mathcal{T}^{\text{ext}} \cdot \bar{\boldsymbol{\eta}} \; d\Gamma = \mathbf{0} \,; \; \forall \, \bar{\boldsymbol{\eta}} \in \bar{\mathcal{V}}_0 \quad (17)$$

where $\bar{\mathbf{B}}$ are the body forces, $\mathcal{T}^{\text{ext}}$ are the external prescribed tractions on the boundary Γ_σ and $\bar{\mathcal{V}}_0$ is the smooth (continuous across $\mathcal{S}$) space of admissible (material) displacement variations. After some algebraic manipulations it is readily obtained from equation (17):

$$\int_{\mathcal{S}} \bar{\boldsymbol{\eta}} \cdot (\mathbf{P}_{\Omega^+} - \mathbf{P}_{\Omega^-}) \cdot \mathbf{N} \; d\Gamma_{\mathcal{S}} = 0 \quad ; \qquad \forall \, \bar{\boldsymbol{\eta}} \in \bar{\mathcal{V}}_0 . \quad (18)$$

whose strong form sets the continuity of the nominal traction $\mathcal{T} = \mathbf{P} \cdot \mathbf{N}$ at both sides of $\mathcal{S}$ in the domain Ω/S:

$$\mathcal{T} = \mathbf{P}_{\Omega^+}|_{\mathbf{X}\in S} \cdot \mathbf{N} = \mathbf{P}_{\Omega^-}|_{\mathbf{X}\in S} \cdot \mathbf{N} \quad (19)$$

In the context of the SDA and the regularized kinematics of section 2.1 we extend, as an "ad hoc" hypothesis, this traction continuity to the interior of the discontinuity interface $\mathcal{S}_h$ of figure 1b:

$$\mathcal{T} = \mathbf{P}_{\Omega^+} \cdot \mathbf{N} = \mathbf{P}_{\Omega^-} \cdot \mathbf{N} = \mathbf{P}_S \cdot \mathbf{N} \quad (20)$$

where $\mathbf{P}_S$ stands for the first Piola-Kirchhoff stress tensor at S. This hypothesis, sustained on the *physical* perception that if there are material points in between Ω^+ and Ω^- the traction continuity (equilibrium) should be also extended to those points, can be retrieved in a more rigorous manner by applying the momentum balance principle (17) to the whole domain Ω and extending the admissible displacements space to $V := \{\boldsymbol{\eta} = \bar{\boldsymbol{\eta}} + \mathcal{H}_S \boldsymbol{\gamma}\}$ according to the kinematics adopted in equation (1)(see reference [29]).

The nominal traction continuity condition (20) has relevant consequences, on the bounded character of the Cauchy stress tensor at the interior of the strong discontinuity band, $\boldsymbol{\sigma}_S$,which emerge from the following reasonings:

1. Since the deformation at $\Omega\backslash S$ is determined by $\bar{\mathbf{F}}$ (that is bounded by definition, according to equation (3)) and the continuum constitutive equation is supposed to return bounded stresses for bounded strains, then the *Piola-Kirchhoff stresses* $\mathbf{P}_{\Omega^+}$ *and* $\mathbf{P}_{\Omega^-}$ *are bounded at any time of the analysis.*

2. If $\mathbf{P}_{\Omega^+}$ and $\mathbf{P}_{\Omega^-}$ are bounded, *so is the nominal traction vector* $\mathcal{T}$ in equation (20) since $\mathbf{N}$ is bounded ($|\mathbf{N}| = 1$).

3. Rewriting the last equation (20) in terms of the Cauchy stresses one gets:

$$\mathcal{T} = \mathbf{P}_S \cdot \mathbf{N} = \boldsymbol{\tau}_S \cdot \mathbf{n} = J\,\boldsymbol{\sigma}_S \cdot \mathbf{n} = \bar{J}\,\boldsymbol{\sigma}_S \cdot \bar{\mathbf{n}} = \bar{J}\,|\bar{\mathbf{n}}|\,\boldsymbol{\sigma}_S \cdot \mathbf{e}_n \qquad (21)$$

   where equations (10) and (12) have been used. In equation (21) $\mathbf{e}_n$ is the unit (and therefore bounded, $\|\mathbf{e}_n\| = 1$) vector parallel to $\mathbf{n}$.

   Since in equation (21) $\mathcal{T}$, $\bar{J}$, and $|\overline{\mathbf{n}}|$are bounded entities, so is the vector $\hat{\mathcal{T}} = \boldsymbol{\sigma}_S \cdot \mathbf{e}_n$ and, since $\boldsymbol{\sigma}_S$ is a symmetric tensor all its components are bounded[3]. Consequently we can state that the *physical stresses at the discontinuous interface,* $\boldsymbol{\sigma}_S$, *are bounded even if the corresponding strains are not.* This fact becomes crucial for the analysis developed in subsequent sections. Observe that the same statement can not, in general, be made for the Kirchhoff stress tensor $\boldsymbol{\tau}_S$.

4. Similar arguments, now on rate entities, lead to *the bounded character of* $\dot{\boldsymbol{\sigma}}_S$. In fact, if $\dot{\mathbf{P}}_{\Omega^+}$ and $\dot{\mathbf{P}}_{\Omega^-}$ are assumed to be bounded on the same above arguments, time derivation of equation (20), considering the material character of S ($\dot{\mathbf{N}} = \mathbf{0}$), leads to the bounded character of $\dot{\mathcal{T}}$. Hence, time derivation of equation (21) read

$$\underbrace{\dot{\mathcal{T}}}_{bounded} = \underbrace{\dot{\bar{J}}}_{bounded}\ \dot{\boldsymbol{\sigma}}_S \cdot \bar{\mathbf{n}} + \underbrace{\dot{\bar{J}}\,\boldsymbol{\sigma}_S \cdot \bar{\mathbf{n}}}_{bounded} + \underbrace{\bar{J}\,\boldsymbol{\sigma}_S \cdot \dot{\bar{\mathbf{n}}}}_{bounded} \qquad (22)$$

[3]This statement comes readily out by expressing the components of equation $\hat{\mathcal{T}} = \boldsymbol{\sigma}_S \cdot \mathbf{e}_n$ in the orthonormal base constituted by the eigenvalues of $\boldsymbol{\sigma}_S$ i.e.: $\hat{\mathcal{T}}_1 = \boldsymbol{\sigma}_1 \hat{n}_1$; $\hat{\mathcal{T}}_2 = \boldsymbol{\sigma}_2 \hat{n}_2$; $\hat{\mathcal{T}}_3 = \boldsymbol{\sigma}_3 \hat{n}_3$ (where $\{\boldsymbol{\sigma}_1, \boldsymbol{\sigma}_2, \boldsymbol{\sigma}_3\}$ are the principal values of $\boldsymbol{\sigma}_S$ and $\{\hat{n}_1, \hat{n}_2, \hat{n}_3\}$ the corresponding components of $\mathbf{e}_n$) and realizing that, since $\hat{\mathcal{T}}_1$, $\hat{\mathcal{T}}_2$,$\hat{\mathcal{T}}_3$,$\hat{n}_1$,$\hat{n}_2$,$\hat{n}_3$ are bounded, those principal values $\boldsymbol{\sigma}_1, \boldsymbol{\sigma}_2, \boldsymbol{\sigma}_3$ are also bounded and, therefore, so are the components of tensor $\boldsymbol{\sigma}_S$ in any base.

where use is made of the bounded character of $\dot{\bar{\mathcal{T}}}$, $\bar{J}, \dot{\bar{J}}, \bar{\mathbf{n}}, \dot{\bar{\mathbf{n}}}$ (from time derivation of the last equation (5)) and $\boldsymbol{\sigma}_S$. Finally, from equation (22) it turns out that $\dot{\boldsymbol{\sigma}}_S \cdot \bar{\mathbf{n}} = \|\bar{\mathbf{n}}\| \dot{\boldsymbol{\sigma}}_S \cdot \mathbf{e}_n$ is bounded and so is $\dot{\boldsymbol{\sigma}}_S \cdot \mathbf{e}_n$. From this, and following the same reasoning as above, the bounded character of $\dot{\boldsymbol{\sigma}}_S$ emerges.

3.2 Development of a strong discontinuity. Weak - strong discontinuities

The regularized kinematics proposed in section 2.1, allows to introduce the *weak discontinuity* concept by considering the same kinematics of equations (7) to (12) but now with a non null bandwidth[4] $h \neq 0$. Bearing these concepts in mind we shall consider the mechanism of formation of a strong discontinuity as follows:

a) At time $t = t_B$ (the *bifurcation time*) a local discontinuous bifurcation of the strain field (see section 3.3) originates a localization of the strains in the shape of a weak discontinuity (with bandwidth $h = h_0$), see figure 2a.

b) A subsequent evolution of the bandwidth $h(t)$, decreasing monotonously along the time, makes that weak discontinuity collapse into a strong one (when the bandwidth reaches a very small regularization value $h \equiv k \to 0$) at time t_{SD} (see figure 2b-c). The bandwidth law is assumed such that the deformation gradient at $t = t_{SD}$ verifies:

$$\lim_{h\to 0} h\mathbf{F}|_{t=t_{SD}} = \lim_{h\to 0} h \int_0^{t=t_{SD}} \left(\dot{\bar{\mathbf{F}}} + \frac{\mu_{\mathcal{S}}}{h} (\llbracket \dot{\mathbf{u}} \rrbracket \otimes \mathbf{N}) \right) dt = \mathbf{0} \qquad (23)$$

For the *strong discontinuity regime* ($t \geq t_{SD}$) the bandwidth is kept constant, $h \equiv k \to 0$, (see figure 2d).

3.3 Bifurcation condition at $t = t_B$

The classical bifurcation analysis [26], [35] determines the conditions for the bifurcation of an initially smooth deformation field to a weak discontinuity

[4] A weak discontinuity can be then characterized by continuous displacements fields and discontinuous (but bounded) strain fields [23].

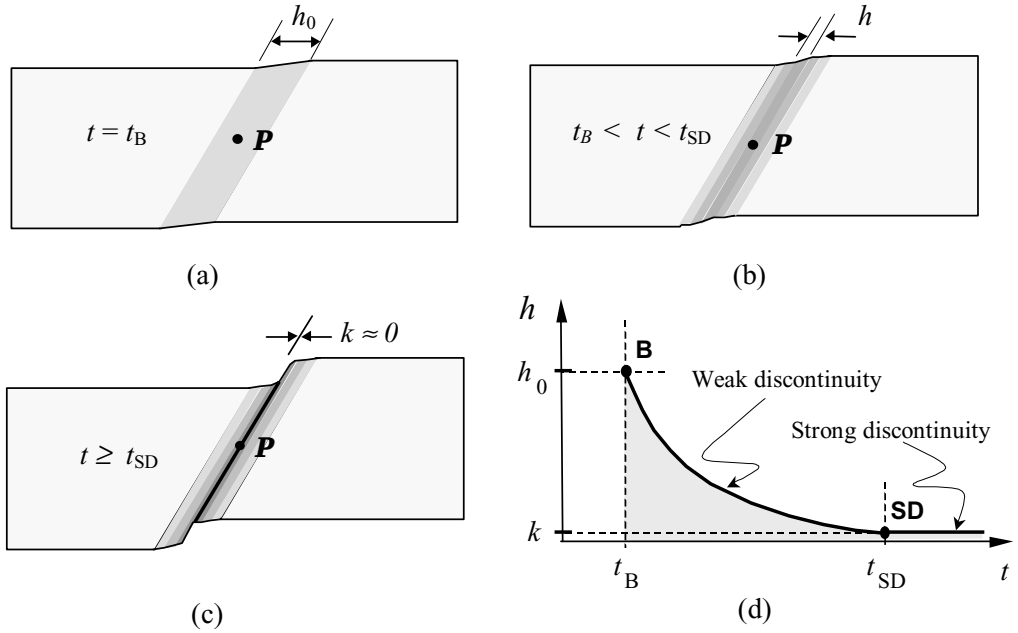

Figure 2: From **(a)** to **(c)** mechanism of formation of a strong discontinuity by collapse of a weak discontinuit; **(d)** variable bandwidth law.

compatible, in turn, with the equilibrium of the body. Therefore, we assume that at time $t = t_B$ a non-smooth deformation rate, described by the rate of the deformation gradient (7), begins developing. The equilibrium condition across the discontinuity surface $\mathcal{S}$ requires the jump of the nominal traction vector to be zero:

$$[\![\dot{\mathcal{T}}]\!] = \left[\dot{\mathbf{P}}(\mathbf{X}_{\mathcal{S}}) - \dot{\mathbf{P}}(\mathbf{X}_{\Omega^+})\right] \cdot \mathbf{N} = \mathbf{0} \tag{24}$$

Assuming loading conditions in $\mathcal{S}$ and neutral loading in $\Omega/\mathcal{S}$[5], and after some algebraic manipulations, it is possible to derive from (24) the following equation [4]:

[5] A preliminary analysis shows that this scenario determines the first (and, therefore, the most unfavorable) possible bifurcation.

$$\mathbf{Q}_{t_B} \cdot [\![\dot{\mathbf{u}}]\!] = \underbrace{\left(\mathbf{e}_n \cdot \mathbf{c}^{\mathrm{tang}} \cdot \mathbf{e}_n + (\mathbf{e}_n \cdot \boldsymbol{\tau} \cdot \mathbf{e}_n)\, \mathbf{1} \right)}_{\mathbf{Q}_{t_B}} \cdot [\![\dot{\mathbf{u}}]\!] = \mathbf{0} \tag{25}$$

where $\mathbf{c}^{\mathrm{tang}}$ is the tangent constitutive tensor, which relates the Kirchhoff stress convective rate with the rate of deformation ($L_v \boldsymbol{\tau} = \mathbf{c}^{\mathrm{tang}} : \mathbf{d}$, see Appendixes I and II for applications to particular models). The criterion to determine bifurcation is based on the detection of the singularity of the localization tensor $\mathbf{Q}_{t_B}$, this allowing a non-trivial solution for the velocity jump ($[\![\dot{\mathbf{u}}]\!] \neq 0$) in equation (25):

$$\det \left[\mathbf{Q}_{t_B}(\mathbf{e}_n, \mathcal{H}^{crit}) \right] = 0 \quad \text{for } t = t_B \tag{26}$$

The first time that equation (26) is fulfilled, for a given material point, determines the bifurcation time t_B for that point, and allows to obtain both the normal $\mathbf{e}_n$, which in turn determines the direction of propagation of the discontinuity interface $\mathcal{S}$, and the initial value of the bandwidth h_0 (see figure 2d) in terms of the critical softening parameter $\mathcal{H}^{crit}$. For further details on this particular procedure the reader is referred to references [35], [22] and [23].

3.4 The continuum and discrete free energies

There is a broad set of continuum constitutive models founded on thermodynamic basis that can be used in finite strain settings. A key point in those models is the definition of the *continuum free energy density function* $\psi(\mathbf{F}, \Gamma)$**,** in terms of the gradient of deformation tensor $\mathbf{F}$, that acts as the *free* (thermodynamically independent) variable, and a set of internal variables Γ (including the inelastic strain measures) characterized by specific evolution laws [14]. The nominal stress field $\mathbf{P}$ can be then directly obtained, on thermodynamical reasonings, from that continuum free energy as:

$$\mathbf{P}(\mathbf{X},t) = \frac{\partial \psi(\mathbf{F}, \Gamma)}{\partial \mathbf{F}} \overset{not}{=} \partial \psi_{\mathbf{F}}(\mathbf{F}, \Gamma) \tag{27}$$

which qualifies the continuum free energy ψ as a potential for the nominal stress field $\mathbf{P}$.

In this context, let us consider the discontinuous interface $\mathcal{S}$ and the free energy per unit of such a surface $\bar{\psi}$, from now on termed the *discrete free energy*, which, in the context of the regularization procedure sketched in section 3.3, can be written as:

$$\bar{\psi} = \tfrac{\text{free energy}}{\text{unit surface}} = \underbrace{\frac{\text{free energy}}{\text{unit volume}}}_{\psi} \cdot \underbrace{\frac{\text{unit volume}}{\text{unit surface}}}_{h} = \lim_{h \equiv \mathbf{k} \to \mathbf{0}} h\psi|_S \tag{28}$$

Now, by considering the strong discontinuity kinematics (8), $\mathbf{F}(\bar{\mathbf{F}}, \boldsymbol{\beta}) = \bar{\mathbf{F}} + \frac{\mu_S}{h}(\boldsymbol{\beta} \otimes \mathbf{N})$, in equation (27) one gets:

$$\left.\begin{aligned} &\bar{\psi}(\bar{\mathbf{F}}, \boldsymbol{\beta}, \Gamma) \equiv \lim_{h \to \mathbf{0}} h\psi_S(\mathbf{F}(\bar{\mathbf{F}}, \boldsymbol{\beta}), \Gamma) \\ &\partial_\beta \bar{\psi} \;\; = \lim_{h \to \mathbf{0}} h\partial_\beta \psi = \lim_{h \to \mathbf{0}} h \;\; \underbrace{\partial_{\mathbf{F}}\psi}_{\mathbf{P}} \cdot \underbrace{\partial_\beta \mathbf{F}}_{\frac{1}{h}\mathbf{N}} \\ &\qquad\quad = \mathbf{P} \cdot \mathbf{N} = \mathcal{T} \end{aligned}\right\} \Rightarrow \boxed{\mathcal{T} = \partial_\beta \bar{\psi}} \tag{29}$$

Equation (29) hints at a crucial consequence of the consideration of strong discontinuous kinematics in continuum (stress-strain) models: projection of those continuum models into discrete (traction-displacement jump) ones. In fact, the discrete free energy $\bar{\psi}$, obtained as the discontinuous surface counterpart of the continuum free energy density ψ, turns into a potential of the nominal traction $\mathcal{T} = \mathbf{P} \cdot \mathbf{N}$, with respect to the incremental jump $\boldsymbol{\beta}$, as shown in equation (29). This suggests that a discrete model can be derived from that discrete free energy and, therefore, from the inclusion of a strong discontinuity kinematics in the original continuum model. Indeed, this is what is shown, for certain representative families of constitutive models (continuum damage and elastoplasticity), in next sections.

3.5 A representative continuum damage model

Let us now consider the extension to the finite deformation range of the isotropic continuum damage model presented in [20]:

Freee energy:	$\psi(\mathbf{b}, r) = (1-d)\psi^0(\mathbf{b})$ $\psi^0(\mathbf{b}) = \frac{1}{4}\lambda\,(J^2-1) - (\frac{\lambda}{2}+\mu)\log J$ $+\frac{1}{2}\mu\;[tr(\mathbf{b})-3]$	(a)
Constitutive equation:	$\mathbf{P} = \partial_{\mathbf{F}}\psi$ $\Updownarrow$ $\boldsymbol{\tau} = 2\mathbf{b}\cdot\partial_{\mathbf{b}}\psi = \frac{q}{r}\left[\lambda\frac{(J^2-1)}{2}\,\mathbf{1} + \mu\,(\mathbf{b}-\mathbf{1})\right]$	(b)
Damage variable:	$d = 1 - \frac{q(r)}{r}\;\;;\quad r \in [0,\infty)$	(c)
Evolution law:	$\dot{r} = \gamma \qquad \begin{cases} r \in [0,\infty) \\ r\vert_{t=0} = r_0 > 0 \end{cases}$	(d)
Damage criterion:	$\phi(\boldsymbol{\sigma}, q) \equiv \tau_\sigma - q \;\;;\qquad \tau_\sigma = \sqrt{\boldsymbol{\sigma}\cdot\mathbf{c}_\phi^{-1}\cdot\boldsymbol{\sigma}}$	(e)
Load.-unl. conditions:	$\gamma \geq 0 \qquad \phi \leq 0 \qquad \gamma\,\phi = 0$	(f)
Softening. rule:	$\dot{q} = \mathcal{H}\dot{r} \;\;;\quad \mathcal{H} < 0 \qquad \begin{cases} q \in [0, r_0] \\ q\vert_{t=0} \overset{not}{=} q_0 = r_0 \end{cases}$	(g)

(30)

where $\mathbf{b}(\mathbf{F}) = \mathbf{F}\cdot\mathbf{F}^T$ is the left Cauchy-Green deformation tensor, r is a scalar strain-like internal variable which determines the damage (or degradation) level of the material and $q(r)$ is a stress-like internal variable that sets the evolution of the elastic domain $\mathrm{E}_\sigma := \{\boldsymbol{\sigma}\;;\,\phi(\boldsymbol{\sigma}, q) < 0\}$ through the damage function $\phi(\boldsymbol{\sigma}, q)$. In addition, in equation (30-(c)), $d(r) = 1 - \frac{q(r)}{r}$ is the classical damage variable ranging from 0 (undamaged state) to 1 (full damage). Also in equation (30-(e)) τ_σ is a norm of the stresses in the metric of the tensor $\mathbf{c}_\phi^{-1}$(see Appendix I for the explicit expression of such a tensor and additional characteristics of the model).

3.5.1 Strong discontinuity analysis

Let us now find out what conditions make the unbounded strains at the strong discontinuity regime, for $t > t_{SD}$ (and thus $h = k \to 0$), compatible with the stress boundedness requirement of section 3.1. Using the multiplicative decomposition (5) and expressions (8) and (10), one can rewrite the Kirchhoff stress (30-b) in the discontinuous interface S as:

$$\begin{aligned}\boldsymbol{\tau}_S &= \frac{q}{r}\left[\frac{\lambda}{2}\left(\bar{J}^2\left[\frac{k+\boldsymbol{\beta}\cdot\bar{\mathbf{n}}}{k}\right]^2-1\right)\mathbf{1}+\mu(\bar{\mathbf{b}}-\mathbf{1})+\right.\\ &\left.+2\mu\left(\frac{\bar{\mathbf{b}}\cdot\bar{\mathbf{n}}\otimes\boldsymbol{\beta}}{k}\right)^{sym}+\mu\frac{\boldsymbol{\beta}\otimes\boldsymbol{\beta}}{k^2}\right]\end{aligned} \tag{31}$$

where $\bar{\mathbf{b}}=\bar{\mathbf{F}}\cdot\bar{\mathbf{F}}^T$. The corresponding Cauchy stresses can be then written, taking into account equations (10) and (11), as:

$$\boldsymbol{\sigma}_S=\frac{1}{J}\boldsymbol{\tau}_S=\frac{q}{r}\left(\boldsymbol{\sigma}_0+\frac{1}{k}\boldsymbol{\sigma}_1\right) \tag{32}$$

where:

$$\boldsymbol{\sigma}_0=-\frac{\lambda}{2\bar{J}}\left(\frac{k}{k+\boldsymbol{\beta}\cdot\bar{\mathbf{n}}}\right)\mathbf{1}+\frac{\mu}{\bar{J}}\left(\frac{k}{k+\boldsymbol{\beta}\cdot\bar{\mathbf{n}}}\right)(\bar{\mathbf{b}}-\mathbf{1}) \tag{33}$$

and

$$\boldsymbol{\sigma}_1=\frac{\lambda}{2}\bar{J}(k+\boldsymbol{\beta}\cdot\bar{\mathbf{n}})\,\mathbf{1}+\frac{\mu}{\bar{J}}\left(\frac{\boldsymbol{\beta}\otimes\boldsymbol{\beta}}{k+\boldsymbol{\beta}\cdot\bar{\mathbf{n}}}\right)+(\frac{2\mu}{\bar{J}})\frac{k}{k+\boldsymbol{\beta}\cdot\bar{\mathbf{n}}}(\bar{\mathbf{b}}\cdot\bar{\mathbf{n}}\otimes\boldsymbol{\beta})^{sym} \tag{34}$$

Now from equations (32) and (34) one can write:

$$\lim_{k\to\mathbf{0}} kr\underbrace{\boldsymbol{\sigma}_S}_{\substack{bounded\\ for\ \ k\to 0}}=q\lim_{k\to\mathbf{0}}(k\underbrace{\boldsymbol{\sigma}_0}_{\substack{bounded\\ for\ \ k\to 0}}+\boldsymbol{\sigma}_1)=\underbrace{q}_{\substack{bounded\\ for\ \ k\to 0}}\lim_{k\to\mathbf{0}}\boldsymbol{\sigma}_1 \tag{35}$$

where the bounded character of $\boldsymbol{\sigma}_S$ (from section 3.1), $\boldsymbol{\sigma}_0$ (from observation of equation (33) and $q\in[0,r_0]$ have been considered. In view of equation (35) we now consider the following two scenarios:

I) $\boxed{\lim_{k\to\mathbf{0}} kr=0}$ (for $t>t_{SD}$):

Then, from equations (34) and (35):

$$\mathbf{0}=\lim_{k\to 0}\boldsymbol{\sigma}_1=\frac{\lambda}{2}\,\bar{J}\,(\boldsymbol{\beta}\cdot\bar{\mathbf{n}})\,\mathbf{1}+\frac{\mu}{\bar{J}\,(\boldsymbol{\beta}\cdot\bar{\mathbf{n}})}(\boldsymbol{\beta}\otimes\boldsymbol{\beta})=\mathbf{0}\quad\Longleftrightarrow\ \boldsymbol{\beta}=\mathbf{0} \tag{36}$$

which states that the incremental displacement jump $\boldsymbol{\beta}$ is null and there is no evolution of the jump at the strong discontinuity regime. Therefore, this scenario would not model the strong discontinuity evolution and has to be discarded. The alternative scenario is then:

II) $\boxed{\lim_{k\to\mathbf{0}} kr \neq 0}$ (for $t > t_{SD}$):

Such condition is trivially fulfilled if we provide the following structure for the evolution of r:

$$\begin{aligned} \dot{r}(t) = \tfrac{\dot{\bar{\alpha}}}{h} \qquad \Rightarrow r \;&=\; \underbrace{\int_0^{t_{SD}} \frac{\dot{\bar{\alpha}}}{h} dt}_{\overset{def}{=} r_{SD}} \; + \int_{t_{SD}}^{t} \tfrac{\dot{\bar{\alpha}}}{k} dt \\ &=\; r_{SD} + \tfrac{1}{k} \quad \underbrace{(\bar{\alpha}_t - \bar{\alpha}_{SD})}_{\overset{def}{=} \Delta\bar{\alpha}} \end{aligned} \tag{37}$$

where $\dot{\bar{\alpha}}$ and $\bar{\alpha}$ are imposed to be bounded and different from zero for $t > t_{SD}$. In fact, from equation (37) it follows that:

$$\begin{aligned} \lim_{k\to\mathbf{0}} kr \;&=\; \underbrace{\lim_{k\to\mathbf{0}} k\, r_{SD}}_{=0} + (\bar{\alpha}_t - \bar{\alpha}_{SD}) \\ &=\; (\bar{\alpha}_t - \bar{\alpha}_{SD}) \overset{def}{=} \Delta\bar{\alpha} \neq 0 \quad \forall t > t_{SD} \end{aligned} \tag{38}$$

Therefore the point is now to guarantee the bounded character of q. Looking at equation (30-(g)) in connection with equation (37):

$$\underbrace{\dot{q}_s}_{bounded} = \mathcal{H} \; \underbrace{\dot{r}_{\,S}}_{\frac{\dot{\bar{\alpha}}}{k}} = \mathcal{H}\,\tfrac{1}{k} \; \underbrace{\dot{\bar{\alpha}}}_{bounded} \quad \Rightarrow \tag{39}$$

$$\mathcal{H}\tfrac{1}{k} = \bar{\mathcal{H}} \text{ (bounded)} \Rightarrow \boxed{\dot{q}_S = \bar{\mathcal{H}}\, \dot{\bar{\alpha}}}$$

Thus, equation (39) is fulfilled from the following *softening regulariza-*

tion condition[6]:

$$\mathcal{H} = h\bar{\mathcal{H}} \quad \forall t \geq t_B \tag{40}$$

where $\bar{\mathcal{H}} < 0$ (from now on termed the *discrete softening parameter*) is a material parameter[7].

Notice that the enforcement of equation (40) implies fulfillment of equations (39) and (38). Therefore, substitution of equation (38) into equation (35) leads finally (in view of equation (34)) to:

$$\begin{gathered} \lim_{k\to 0}(kr\,\boldsymbol{\sigma}_S) = \Delta\bar{\alpha}\,\boldsymbol{\sigma}_S = q\,\boldsymbol{\sigma}_1 \Rightarrow \\ \boldsymbol{\sigma}_S(\boldsymbol{\beta}) = \tfrac{q}{\Delta\bar{\alpha}}\lim_{k\to 0}\boldsymbol{\sigma}_1 = \tfrac{q}{\Delta\bar{\alpha}}\left[\tfrac{\lambda}{2}\bar{J}(\boldsymbol{\beta}\cdot\bar{\mathbf{n}})\,\mathbf{1} + \mu\tfrac{1}{\bar{J}\boldsymbol{\beta}\cdot\bar{\mathbf{n}}}\boldsymbol{\beta}\otimes\boldsymbol{\beta}\right] \end{gathered} \tag{41}$$

Equation (41) provides a set of six (due to symmetry) equations that allow to solve for the incremental jump $\boldsymbol{\beta}$ (three equations) and supplies three constrains on the stress field $\boldsymbol{\sigma}_S$. In fact by multiplying such equation times $\mathbf{n}$ one obtains:

$$\mathcal{T} = J\boldsymbol{\sigma}_S\cdot\mathbf{n} = \bar{J}\,\boldsymbol{\sigma}_S\cdot\bar{\mathbf{n}} = \tfrac{q}{\Delta\bar{\alpha}}\ \underbrace{\left(\frac{\lambda}{2}\bar{J}^2(\bar{\mathbf{n}}\otimes\bar{\mathbf{n}}) + \mu\,\mathbf{1}\right)}_{\mathbf{Q}\ \left(\bar{J}\,\bar{\mathbf{n}}\right)}\cdot\boldsymbol{\beta} \Rightarrow \tag{42}$$

$$\boxed{\mathcal{T} = (1-\omega)\mathbf{Q}\cdot\boldsymbol{\beta}\ ; \qquad \omega = 1 - \tfrac{q}{\Delta\bar{\alpha}}\ ; \quad \omega\in[-\infty,1]} \tag{43}$$

that can clearly be interpreted as a *discrete damage law* for the cohesive interface. It describes the relation between the traction $\mathcal{T}$ and the displacement jump $\boldsymbol{\beta}$ in terms of a discrete damage variable $\omega\in[-\infty,1]$[8] and an *acoustic*-like stiffness tensor $\mathbf{Q}$. In turn, equation (43) can

[6] In strict sense the softening regularization condition is only required at the strong discontinuity regime ($\mathcal{H} = k\bar{\mathcal{H}} \quad \forall t \geq t_{SD}$) but, in the context of the variable bandwidth model, it is also extended to the weak discontinuity regime ($t_B \leq t < t_{SD}$) (see references [22] and [23]).

[7] In fact the discrete softening parameter $\bar{\mathcal{H}}$ can be readly related to the fracture energy concept in fracture mechanics[20].

[8] The initial $\omega = -\infty$ value states that the induced discrete model is a *rigid* damage model. This extends to finite deformation settings this feature already proved for infinitesimal strains settings [20].

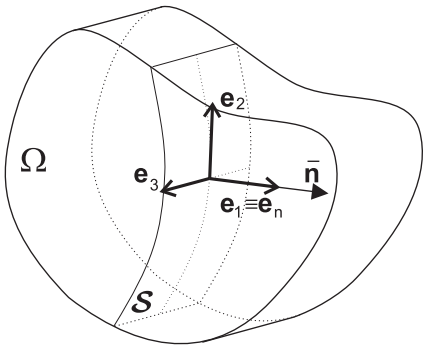

Figure 3: Orthogonal basis attached to the discontinuity surface.

be solved for $\boldsymbol{\beta}$ ($\boldsymbol{\beta} = \frac{\Delta\bar{\alpha}}{q}\mathbf{Q}^{-1}\cdot\mathcal{T}$) and, once substituted into equation (41), provides a set of three equations in terms of $\boldsymbol{\sigma}_S$, which are termed the *strong discontinuity conditions* [20], that have to be fulfilled at the strong discontinuity regime ($t \geq t_{SD}$). In a local orthogonal basis $(\mathbf{e}_1, \mathbf{e}_2, \mathbf{e}_3)$, see figure 3, with unit vectors $\mathbf{e}_2$ and $\mathbf{e}_3$ laying on the tangent plane to the discontinuity surface, $\mathcal{S}$, and $\mathbf{e}_1 = \mathbf{n}/\|\mathbf{n}\| = \bar{\mathbf{n}}/\|\bar{\mathbf{n}}\|$, they can be written as:

$$\left.\begin{aligned} \sigma_{22} &= \tfrac{\hat{\lambda}}{\mu+\hat{\lambda}}\sigma_{11} + \tfrac{\mu+\hat{\lambda}}{\mu}(\sigma_{12}^2/\sigma_{11}) \\ \sigma_{33} &= \tfrac{\hat{\lambda}}{\mu+\hat{\lambda}}\sigma_{11} + \tfrac{\mu+\hat{\lambda}}{\mu}(\sigma_{13}^2/\sigma_{11}) \\ \sigma_{23} &= \tfrac{\mu+\hat{\lambda}}{\mu}(\sigma_{12}\sigma_{13}/\sigma_{11}) \\ & (\hat{\lambda} = \tfrac{\lambda}{2}\bar{J}^2\,\|\bar{\mathbf{n}}\|^2) \end{aligned}\right\} \quad \forall t \geq t_{SD} \tag{44}$$

which states an explicit non-linear functional dependence of the stress σ_{22}, σ_{33} and σ_{23} on the traction vector components $[\mathcal{T}] \equiv [\sigma_{11}, \sigma_{12}, \sigma_{13}]$. Therefore the strong discontinuity conditions impose a particular stress state at the discontinuous interface $\mathcal{S}$ that make it directly dependent on the traction $\mathcal{T}$ i.e.:

$$\boldsymbol{\sigma}_S = \boldsymbol{\sigma}_S(\mathcal{T}) \qquad \forall t \geq t_{SD} \tag{45}$$

Now recalling the expression of the discrete free energy (28) for the particular case of equations (30a) one obtains, after some algebraic

manipulation:

$$\lim_{k\to 0} k\psi(\mathbf{b}, r) = \bar{\psi}(\boldsymbol{\beta}, \bar{\mathbf{n}}, \Delta\bar{\alpha}) \tag{46}$$

$$\bar{\psi}(\boldsymbol{\beta}, \bar{\mathbf{n}}, \Delta\bar{\alpha}) = \frac{q(\Delta\bar{\alpha})}{\Delta\bar{\alpha}}\bar{\psi}^0(\boldsymbol{\beta}, \bar{\mathbf{n}}) \; ; \quad \bar{\psi}^0 = \frac{\lambda}{4}\bar{J}^2(\boldsymbol{\beta}\cdot\bar{\mathbf{n}})^2 + \mu(\boldsymbol{\beta}\cdot\boldsymbol{\beta}) \tag{47}$$

and, from the expression of the discrete free energy (47), the constitutive equation (42) is immediately recovered by derivation ($\mathcal{T} = \partial_{\beta}\bar{\psi}$), as suggested in section 3.4. From that, the following discrete constitutive model can be finally obtained:

Freee energy:	$\bar{\psi}(\beta, \Delta\bar{\alpha}) = (1-\omega)\bar{\psi}^0$ $\bar{\psi}^0(\boldsymbol{\beta}) = \frac{\lambda}{4}\bar{J}^2(\boldsymbol{\beta}\cdot\bar{\mathbf{n}})^2 + \mu(\boldsymbol{\beta}\cdot\boldsymbol{\beta})$	(a)
Constitutive equation:	$\mathcal{T} = \partial_{\beta}\psi = (1-\omega)\mathbf{Q}\cdot\boldsymbol{\beta}$ $\mathbf{Q}(\bar{J}\bar{\mathbf{n}}) = \frac{\lambda}{2}\bar{J}^2(\bar{\mathbf{n}}\otimes\bar{\mathbf{n}}) + \mu\,\mathbf{1}$	(b)
Damage variable:	$\omega = 1 - \frac{q(\Delta\bar{\alpha})}{\Delta\bar{\alpha}}$; $\quad \omega \in (-\infty, 1]$	(c)
Evolution law:	$\dot{\alpha} = \bar{\gamma}$; $\left\{\begin{array}{c}\Delta\bar{\alpha} \in [0,\infty) \\ \Delta\bar{\alpha}\vert_{t_{SD}} = 0\end{array}\right.$	(d)
Damage criterion:	$\phi(\mathcal{T}, q) = \tau_{\mathcal{T}} - q_S$ $\tau_{\mathcal{T}} = \sqrt{\boldsymbol{\sigma}_S(\mathcal{T})\cdot\mathbf{c}_{\phi}^{-1}\cdot\boldsymbol{\sigma}_S(\mathcal{T})}$	(e)
Load.-unl. conditions:	$\bar{\gamma} \geq 0 \quad \bar{\phi} \leq 0 \quad \bar{\gamma}\,\bar{\phi} = 0$	(f)
Softening. rule:	$\dot{q}_S = \bar{\mathcal{H}}\,\dot{\bar{\alpha}}\,;\ \bar{\mathcal{H}} < 0\,;$ $\left\{\begin{array}{c} q_S \in [0, q_{SD}] \\ q_{SD} \overset{not}{=} q_S\vert_{t_{SD}}\end{array}\right.$	(g)

(48)

3.6 A representative elastoplastic model

As a second family of constitutive equations let us consider those isotropic elastoplastic models based on the multiplicative decomposition of the deformation gradient in the elastic and a plastic counterparts [14]:

$$\mathbf{F} = \mathbf{F}^e \cdot \mathbf{F}^p \tag{49}$$

such that the spatial velocity gradient ($\mathbf{l}$) the rate of deformation ($\mathbf{d}$) and the spin ($\mathbf{w}$) tensors are evaluated as :

$$\mathbf{l} = \mathbf{l}^e + \mathbf{l}^p \; ; \qquad \mathbf{d} = \mathbf{l}^{\text{sym}} = \mathbf{d}^e + \mathbf{d}^p \; ; \qquad \mathbf{w} = \mathbf{l}^{\text{skw}} = \mathbf{w}^e + \mathbf{w}^p \tag{50}$$

with

$$\mathbf{l}^e = \dot{\mathbf{F}}^e \cdot \mathbf{F}^{e-1} \; ; \qquad \mathbf{l}^p = \mathbf{F}^e \cdot \dot{\mathbf{F}}^p \cdot \mathbf{F}^{p-1} \cdot \mathbf{F}^{e-1} = \mathbf{F}^e \cdot \mathbf{L}^p \cdot \mathbf{F}^{e-1} \tag{51}$$

$$\mathbf{d}^p = \left[\mathbf{F}^e \cdot (\mathbf{L}^p) \cdot \mathbf{F}^{e-1}\right]^{\mathrm{sym}} \; ; \qquad \mathbf{w}^p = [\mathbf{F}^e \cdot \mathbf{L}^p \cdot \mathbf{F}^{e-1}]^{\mathrm{skw}} \tag{52}$$

A particular model belonging to such a family is the J_2 plasticity model with isotropic hardening described through the following ingredients ([30], [27]):

Freee energy:	$\psi(\mathbf{F}, \mathbf{F}^p, \alpha) = \psi^e(\mathbf{b}^e) + \mathsf{H}^p(\alpha)$ $\begin{cases} \psi^e(\mathbf{b}^e) = \frac{1}{2}\lambda \; tr^2(Ln\sqrt{\mathbf{b}^e}) \\ \qquad\qquad +\mu \;\; Ln\sqrt{\mathbf{b}^e} : Ln\sqrt{\mathbf{b}^e} \\ \mathsf{H}^p(\alpha) = \frac{1}{2}\mathcal{H}\alpha^2 \end{cases}$ $(\mathbf{b}^e = \mathbf{F}^e \cdot \mathbf{F}^{eT})$	(a)
Constitutive equation:	$\mathbf{P} = \partial_{\mathbf{F}}\psi = \partial^e_{\mathbf{F}}\psi \iff$ $\boldsymbol{\tau} = 2\mathbf{b}^e \cdot \partial_{\mathbf{b}^e}\psi^e$ $= \lambda tr(Ln\sqrt{\mathbf{b}^e})\,\mathbf{1} + 2\mu(Ln\sqrt{\mathbf{b}^e})$ $\Leftrightarrow L^e_v\boldsymbol{\tau} = \mathbf{c}^e : \mathbf{d}^e = \mathbf{c}^e : (\mathbf{d} - \mathbf{d}^p)$	(b)
Plastic flow rule:	$\mathbf{d}^p = \gamma\,\mathbf{m} \quad ; \qquad \mathbf{m} = \partial_{\boldsymbol{\tau}}\phi = \sqrt{\frac{3}{2}}\frac{\mathrm{dev}(\boldsymbol{\tau})}{\|\mathrm{dev}(\boldsymbol{\tau})\|}$	(c)
Evolution law:	$\dot{\alpha} = \gamma \qquad \begin{cases} \alpha \in [0, \infty) \\ \alpha\big\|_{t=0} = 0 \end{cases}$	(d)
Yield criterion:	$\phi(\boldsymbol{\tau}, q) \equiv \hat{\phi}(\boldsymbol{\tau}) - (\tau_y + q)$ $\hat{\phi}(\boldsymbol{\tau}) = \sqrt{\frac{3}{2}}\,\|\mathrm{dev}(\boldsymbol{\tau})\|$	(e)
Load.-unl. conditions:	$\gamma \geq 0 \qquad \phi \leq 0 \qquad \gamma\,\phi = 0$	(f)
Softening. rule:	$q = \partial_\alpha \mathsf{H}^p(\alpha) \qquad \begin{cases} q \in [0, \tau_y] \\ q\big\|_{t=0} \overset{not}{=} q_0 = \tau_y \end{cases}$ $\dot{q} = \partial_{\alpha\alpha}\mathsf{H}^p(\alpha)\,\dot{\alpha} = \mathcal{H}\dot{\alpha}$	(g)

(53)

where $\psi^e(\mathbf{b}^e)$ and $\mathsf{H}^p(\alpha)$ are, respectively, the elastic and plastic counterparts of the free energy and α is the scalar strain-like internal variable, $L^e_v(\cdot)$ is the Lie derivative associated to the motion represented by $\mathbf{F}^e$, $\boldsymbol{\tau}$ stands for the Kirchhoff stress ($\mathrm{dev}(\boldsymbol{\tau})$ being its deviatoric counterpart) and $\mathbf{c}^e$ is the elastic constitutive tensor relating the stress rate $L^e_v(\boldsymbol{\tau})$ with the elastic deformation rate $\mathbf{d}^e$. In equation (53e) $\hat{\phi}(\boldsymbol{\tau})$ is the uniaxial equivalent Kirchhoff stress and, therefore, the plastic flow tensor $\mathbf{m} = \partial_{\boldsymbol{\tau}}\hat{\phi}$, in equation

(53c), is non-dimensional and bounded. Moreover q is the scalar stress-like internal hardening variable, $\mathcal{H} < 0$ is the continuum softening parameter and τ_y and γ are, respectively, the yield stress and the plastic multiplier.

In addition to the equations (53) the evolution of the term $\mathbf{w}^p$ can be written as:

$$\mathbf{w}^p = \boldsymbol{\gamma}\,\hat{\mathbf{w}}(\boldsymbol{\tau}) \;\Rightarrow\; \mathbf{l}^p = \mathbf{d}^p + \mathbf{w}^p = \gamma \underbrace{(\mathbf{m} + \hat{\mathbf{w}})}_{\overset{not}{=}\,\hat{\mathbf{l}}} = \gamma\,\hat{\mathbf{l}} \tag{54}$$

For this family of isotropic models with scalar internal variable, this evolution law does not play any role in the constitutive model, resulting τ independent from $\mathbf{w}^p$ and, therefore, from $\hat{\mathbf{w}}$ (by assuming $\hat{\mathbf{w}} = \mathbf{0}$, the above model results the same one as that presented in ([30], [27])). For convenience, here we adopt an arbitrary, but bounded, not null value for $\hat{\mathbf{w}}$. Additional details on this model can be found in Appendix II, where the integration algorithm for the constitutive equation is also shown.

3.6.1 Strong discontinuity analysis

Like in the damage model case, let us investigate what conditions make the elastoplastic model of equation (53) compatible with the strong discontinuity kinematics and the stress boundedness conditions stated in section 3.1. The analysis is based on the following algebraic identities:

- From the identities $L_v\,\boldsymbol{\tau} = \dot{\boldsymbol{\tau}} - \mathbf{l}\cdot\boldsymbol{\tau} - \boldsymbol{\tau}\cdot\mathbf{l}^T$ and $\boldsymbol{\tau} = J\boldsymbol{\sigma}$ ([31]) some trivial operations lead to:

$$L_v\,\boldsymbol{\tau} = L_v\,(J\boldsymbol{\sigma}) = J\left[\,tr(\mathbf{l})\,\boldsymbol{\sigma} + \dot{\boldsymbol{\sigma}} - \mathbf{l}\cdot\boldsymbol{\sigma} - \boldsymbol{\sigma}\cdot\mathbf{l}^T\right] \tag{55}$$

- From the identity $L_v\,\boldsymbol{\tau} = L^e_v\boldsymbol{\tau} - \mathbf{l}^p\cdot\boldsymbol{\tau} - \boldsymbol{\tau}\cdot\mathbf{l}^{pT}$, the constitutive equation (53-b) ($L^e_v\boldsymbol{\tau} = \mathbf{c}^e : \mathbf{d}^e = \mathbf{c}^e : (\mathbf{d} - \mathbf{d}^p)$) the plastic flow rule (53c) ($\mathbf{d}^p = \gamma\,\mathbf{m}$) and equation(54) one gets:

$$\begin{aligned} L_v\,\boldsymbol{\tau} &= L^e_v\boldsymbol{\tau} - (\mathbf{l}^p\cdot\boldsymbol{\tau} + \boldsymbol{\tau}\cdot\mathbf{l}^p) \\ &= \mathbf{c}^e : \mathbf{d} - \gamma\left[\mathbf{c}^e : \mathbf{m} + J\,\hat{\mathbf{l}}\cdot\boldsymbol{\sigma} + J\boldsymbol{\sigma}\cdot\hat{\mathbf{l}}^T\right] \end{aligned} \tag{56}$$

Let us now consider the following particular times for the strong discontinuity regime ($t \geq t_{SD}$):

a) $\boxed{t = t_{SD}}$ (the strong discontinuity time) characterized, therefore, by a null value of the incremental displacement jump ($\boldsymbol{\beta} = \mathbf{0}$, see equation (4b)). In consequence the following identities fulfill from the equations in section 2.1:

$$\begin{aligned} & J = \bar{J}\,(bounded) \Rightarrow \lim_{h \equiv \mathbf{k} \to \mathbf{0}} kJ = 0 \\ & \mathbf{l} = \overline{\mathbf{l}} + \tfrac{\mu_S}{h}\,(\bar{L}_{\bar{v}}\boldsymbol{\beta} \otimes \bar{\mathbf{n}}) \Rightarrow \lim_{h \equiv \mathbf{k} \to \mathbf{0}} k\,\mathbf{l} = \mu_S\,(\bar{L}_{\bar{v}}\boldsymbol{\beta} \otimes \bar{\mathbf{n}}) \\ & \lim_{k \to \mathbf{0}} k\,\mathbf{d} = \lim_{k \to \mathbf{0}} k\,\mathbf{l}^{sym} = \mu_S\,(\bar{L}_{\bar{v}}\boldsymbol{\beta} \otimes \bar{\mathbf{n}})^{sym} \\ & \lim_{k \to \mathbf{0}} k\,tr(\mathbf{l}) = \lim_{k \to \mathbf{0}} \mu_S\ tr(\bar{L}_{\bar{v}}\boldsymbol{\beta} \otimes \bar{\mathbf{n}}) = \mu_S(\bar{L}_{\bar{v}}\boldsymbol{\beta} \cdot \bar{\mathbf{n}}) \end{aligned} \tag{57}$$

Bearing these results in mind, by equating expressions (55) and (56) for a given point on $\mathcal{S}$, multiplying both sides of the equality times $\bar{\mathbf{n}}$, and taking the limit for the strong discontinuity regime ($h \equiv k \to 0$) one gets, in view of equation (57):

$$\underbrace{\left[\bar{\mathbf{n}} \cdot \mathbf{c}^e \cdot \bar{\mathbf{n}} + \bar{J}\ (\bar{\mathbf{n}} \cdot \boldsymbol{\sigma}_S \cdot \bar{\mathbf{n}})\right]}_{\mathbf{Q}^e} \cdot \bar{L}_{\bar{v}}\boldsymbol{\beta} = \mathbf{Q}^e \cdot \bar{L}_{\bar{v}}\boldsymbol{\beta} = (\lim_{k \to \mathbf{0}} k\gamma)\ \mathbf{r} \tag{58}$$

where the bounded character of $\boldsymbol{\sigma}_S$ and $\dot{\boldsymbol{\sigma}}_S$ (and, thus, $\lim_{k \to \mathbf{0}} k\boldsymbol{\sigma}_S = \lim_{k \to \mathbf{0}} k\dot{\boldsymbol{\sigma}}_S = \mathbf{0}$) has been considered. For the most common case, tensor $\mathbf{Q}^e$ is positive definite[9] ($det\mathbf{Q}^e > 0$) and the following two options can be considered in equation (58):

1) $\lim_{k \to \mathbf{0}} k\gamma = 0$ (γ bounded).Thus, since $\mathbf{r}$ is bounded, equation (58) reads $\mathbf{Q}^e \cdot \bar{L}_{\bar{v}}\boldsymbol{\beta} = \mathbf{0}$ and thus $\bar{L}_{\bar{v}}\boldsymbol{\beta} = \mathbf{0}$ precluding any evolution of the jump at the strong discontinuity time t_{SD} (and the corresponding bifurcation stated in Section 3.3). In consequence this possibility should be discarded and *the only feasible option is*:

[9] Under the reasonable assumption, for normal materials, that the stress magnitudes (characterized by the yield stress value τ_y) are smaller in comparison with the elastic parameters λ and μ it can be shown that the tensor $\mathbf{Q}^e = \bar{\mathbf{n}} \cdot \mathbf{c}^e \cdot \bar{\mathbf{n}} + \bar{J}(\bar{\mathbf{n}} \cdot \boldsymbol{\sigma}_S \cdot \bar{\mathbf{n}})\,\mathbf{1}$ is positive definite.

2) $\lim_{k\to\mathbf{0}} k\gamma = \bar{\gamma} \neq 0$ ($\gamma = O(\frac{1}{k})$ = unbounded). Although, according to the previous reasoning, this condition is only required at the strong discontinuity time ($t = t_{SD}$), we shall extend it to the whole strong discontinuity regime, i.e.:

$$\lim_{k\to\mathbf{0}} k\gamma = \bar{\gamma} \neq 0 \quad \forall t \geq t_{SD} \tag{59}$$

b) $\boxed{t_{SD} < t < \infty.}$ For any time in this range, and with regard to the normal component of the incremental jump ($\beta_n = \boldsymbol{\beta} \cdot \bar{\mathbf{n}}$), two possibilities appear:

Case b-1 $\boxed{\boldsymbol{\beta} \cdot \bar{\mathbf{n}} \neq 0}$. Now the following identities fulfill from the equations in section 2.1:

$$\begin{aligned}
&J = \bar{J}(1 + \tfrac{\boldsymbol{\beta}\cdot\bar{\mathbf{n}}}{h}) \;\; (\textit{unbounded}) \Rightarrow \lim_{h\equiv\mathbf{k}\to\mathbf{0}} kJ = \bar{J}\,\boldsymbol{\beta}\cdot\bar{\mathbf{n}} \\
&\mathbf{l} = \bar{\mathbf{l}} + \tfrac{\mu_S}{h+\boldsymbol{\beta}\cdot\bar{\mathbf{n}}}\,(\bar{L}_{\bar{v}}\boldsymbol{\beta}\otimes\bar{\mathbf{n}}) \;\; (\textit{bounded}) \Rightarrow \lim_{h\equiv\mathbf{k}\to\mathbf{0}} (k\,\mathbf{l}) = \mathbf{0} \\
&\lim_{h\equiv\mathbf{k}\to\mathbf{0}} k\mathbf{d} = \lim_{h\equiv\mathbf{k}\to\mathbf{0}} k\,\mathbf{l}^{sym} = \mathbf{0} \\
&\lim_{h\equiv\mathbf{k}\to\mathbf{0}} k\,tr(\mathbf{l}) = 0
\end{aligned} \tag{60}$$

By equating expressions (55) and (56), multiplying both sides times k^2 and taking the limit for the strong discontinuity regime ($h \equiv k \to 0$), in view of equations (59) and (60), one obtains:

$$\begin{aligned}
\lim_{k\to\mathbf{0}} k^2\,L_v\,\boldsymbol{\tau}_S \;\; &= \;\; \lim_{k\to\mathbf{0}} \underbrace{kJ}_{\bar{J}\,\beta\cdot\bar{n}}\; \underbrace{k\,\left[\,tr(\mathbf{l})\,\boldsymbol{\sigma}_S + \dot{\boldsymbol{\sigma}}_S - \mathbf{l}\cdot\boldsymbol{\sigma}_S - \boldsymbol{\sigma}_S\cdot\mathbf{l}^T\right]}_{=0} \\
&= \;\; \mathbf{0} = \lim_{k\to\mathbf{0}}(\; \underbrace{k^2\,\mathbf{c}^e : \mathbf{d}}_{=\,0} - \underbrace{k\gamma}_{=\bar{\gamma}}\,[\underbrace{k\mathbf{c}^e : \mathbf{m}}_{=0} + \\
&\qquad \underbrace{kJ}_{\bar{J}\,\beta\cdot\bar{n}}\,(\hat{\mathbf{l}}\cdot\boldsymbol{\sigma}_S + \boldsymbol{\sigma}_S\cdot\hat{\mathbf{l}}^T)\,]\;)
\end{aligned} \tag{61}$$

$$\Rightarrow \;\; \underbrace{\bar{J}\;(\boldsymbol{\beta}\cdot\bar{\mathbf{n}})\;\bar{\gamma}}_{\neq\,0} \;\; (\hat{\mathbf{l}}\cdot\boldsymbol{\sigma}_S + \boldsymbol{\sigma}_S\cdot\hat{\mathbf{l}}^T) = \mathbf{0} \Rightarrow \tag{62}$$

$$\hat{\mathbf{l}}\cdot\boldsymbol{\sigma}_S + \boldsymbol{\sigma}_S\cdot\hat{\mathbf{l}}^T = \mathbf{0}$$

and, taking into account equation (54), equation (62) reads:

$$\begin{aligned} \hat{\mathbf{l}} \cdot \boldsymbol{\sigma}_S + \boldsymbol{\sigma}_S \cdot \hat{\mathbf{l}}^T &= [\mathbf{m}(\boldsymbol{\sigma}_S) + \hat{\mathbf{w}}] \cdot \boldsymbol{\sigma}_S \\ &\quad + \boldsymbol{\sigma}_S \cdot [\mathbf{m}(\boldsymbol{\sigma}_S) + \hat{\mathbf{w}}]^T = \mathbf{0} \quad \forall \hat{\mathbf{w}} \end{aligned} \tag{63}$$

where the fact that $\boldsymbol{\sigma}_S$ is independent of $\mathbf{w}^p$, described by $\hat{\mathbf{w}}$**,** is emphasized. Consequently, the arbitrary value of $\hat{\mathbf{w}}$ in equation (62) makes $\boldsymbol{\sigma}_S = \mathbf{0}$ the only possible solution for such equation and, therefore, we conclude that *the trial condition* $\boldsymbol{\beta} \cdot \bar{\mathbf{n}} \neq 0$ *must be discarded and the only feasible option is:*

Case b-2 $\boxed{\boldsymbol{\beta} \cdot \bar{\mathbf{n}} = 0}$. Now again equations (57) hold from substitution of condition $\boldsymbol{\beta} \cdot \bar{\mathbf{n}} = 0$ in the ones in section 2.1. In addition, since $\boldsymbol{\beta} \cdot \bar{\mathbf{n}} = 0 \quad \forall t \geq t_{SD}$ then:

$$\begin{aligned} 0 = \tfrac{d}{dt}(\boldsymbol{\beta} \cdot \bar{\mathbf{n}}) = \bar{L}_{\bar{v}} \boldsymbol{\beta} \cdot \bar{\mathbf{n}} + \boldsymbol{\beta} \cdot \underbrace{\bar{L}_{\bar{v}} \bar{\mathbf{n}}}_{F \cdot N = 0} \\ \Rightarrow \boxed{\bar{L}_{\bar{v}} \boldsymbol{\beta} \cdot \bar{\mathbf{n}} = 0 \; \forall t \geq t_{SD}} \end{aligned} \tag{64}$$

that precludes the development of the normal component of the jump $\boldsymbol{\beta} \cdot \bar{\mathbf{n}}$. Therefore *only mode II type discontinuities (tangential displacement jumps) can be modelled using the plasticity model in equation* (53). This restriction is also found for infinitesimal deformation settings for J2-type plasticity models[10] [20].

As we have seen above the obtention of the results in equation (64) lies crucially on the fulfillment of the plastic multiplier regularization condition (59), that, in view of equation (53d), can be rewritten as:

$$\lim_{k \to \mathbf{0}} k \, \dot{\alpha} = \bar{\gamma} \neq 0 \quad \forall t \geq t_{SD} \tag{65}$$

In an manner analogous to equations (37) to (40), for the damage model, such condition is fulfilled if the following structure is

[10] Here in fact, and according to the preceeding reasonings, this result is unaffected by the chosen flow rule (and it holds for any definition of the flow tensor $\mathbf{m}$). Therefore, unlike the infinitesimal strain case, in large strain settings this result is not only restricted to J_2 plasticity models.

provided to the evolution of the continuum internal variable α :

$$\dot{\alpha} = \frac{\dot{\bar{\alpha}}}{h} \Rightarrow \lim_{h \equiv \mathbf{k} \to \mathbf{0}} k\, \dot{\alpha} = \bar{\gamma} = \dot{\bar{\alpha}} \quad \Rightarrow$$

$$\alpha = \underbrace{\int_0^{t_{SD}} \frac{\dot{\bar{\alpha}}}{h} dt}_{\stackrel{def}{=} \bar{\alpha}_{SD}} + \int_{t_{SD}}^{t} \frac{\dot{\bar{\alpha}}}{k} dt = \bar{\alpha}_{SD} + \frac{1}{k} \underbrace{(\bar{\alpha}_t - \bar{\alpha}_{SD})}_{\stackrel{def}{=} \Delta\, \bar{\alpha}} \tag{66}$$

$\bar{\alpha}$ and $\dot{\bar{\alpha}}$ being bounded and different from zero for $t > t_{SD}$. Looking now at the evolution equation (53g) for the softening variable q[11]:

$$\underbrace{\dot{q}_S}_{bounded} = \mathcal{H} \underbrace{\dot{\alpha}}_{\frac{\dot{\bar{\alpha}}}{k}} = \mathcal{H} \frac{1}{k} \underbrace{\dot{\bar{\alpha}}}_{bounded} \Rightarrow \mathcal{H}\frac{1}{k} = \bar{\mathcal{H}} \text{ (bounded)}$$

$$\boxed{\dot{q}_S = \bar{\mathcal{H}}\, \dot{\bar{\alpha}}} \tag{67}$$

where $\bar{\mathcal{H}}$ stands for *the intrinsic or discrete softening parameter,* we arrive again to the softening regularization condition:

$$\mathcal{H} = h\bar{\mathcal{H}} \tag{68}$$

as a *sufficient* condition to make consistent the preceeding analysis. In view of equations (53d) and (66) this softening regularization condition translates into the following regularization of the plastic multiplier:

$$\gamma = \dot{\alpha} = \frac{1}{h}\, \dot{\bar{\alpha}} = \frac{1}{h} \bar{\gamma} \tag{69}$$

On the other hand, by equating expressions (55) and (56), multiplying both sides times k and taking the limit for the strong discontinuity regime ($h \equiv k \to 0$), in view of equations (57) and

[11] The bounded character of q_S comes from the condition $q \in [0, \tau_y]$. The bounded character of $\dot{q}_S$ lies on the bounded character of σ_S and $\dot{\sigma}_S$ (and therefore of $\tau_S = \bar{J}\, \sigma_S$ and $\dot{\tau}_S$) and the consistency condition: $\dot{\phi}(\boldsymbol{\tau}_S) = 0 \Rightarrow \dot{q}_S = \mathbf{m}(\boldsymbol{\tau}_S) : \dot{\boldsymbol{\tau}}_S = (bounded)$

(64) the result reads:

$$\begin{aligned}\lim_{k\to\mathbf{0}} kL_v\,\boldsymbol{\tau}_S &= \bar{J}\,(\underbrace{\bar{L}_{\bar{v}}\boldsymbol{\beta}\cdot\bar{\mathbf{n}}}_{=0})\,\boldsymbol{\sigma}_S \\ &\quad - \underbrace{\bar{J}\,(\bar{L}_{\bar{v}}\boldsymbol{\beta}\otimes\bar{\mathbf{n}}\cdot\boldsymbol{\sigma}_S + \boldsymbol{\sigma}_S\cdot\bar{\mathbf{n}}\otimes\bar{L}_{\bar{v}}\boldsymbol{\beta})}_{2(\bar{L}_{\bar{v}}\beta\otimes T)^{\mathrm{sym}}} \\ &= \mathbf{c}^e : (\bar{L}_{\bar{v}}\boldsymbol{\beta}\otimes\bar{\mathbf{n}})^{sym} \\ &\quad - \underbrace{k\gamma}_{=\bar{\gamma}}\left[\mathbf{c}^e : \mathbf{m}_S + \bar{J}(\hat{\mathbf{l}}\cdot\boldsymbol{\sigma}_S + \boldsymbol{\sigma}_S\cdot\hat{\mathbf{l}}^T)\right]\end{aligned} \tag{70}$$

and, reordering terms, one gets:

$$\begin{aligned}(\bar{L}_{\bar{v}}\boldsymbol{\beta}\otimes\bar{\mathbf{n}})^{sym} &= \bar{\gamma}\mathbf{m}_S - \mathbf{c}^{e-1} : \underbrace{2\,[(\bar{L}_{\bar{v}}\boldsymbol{\beta}\otimes\mathcal{T})^{\mathrm{sym}} - \bar{\gamma}\bar{J}(\hat{\mathbf{l}}\cdot\boldsymbol{\sigma}_S)^{\mathrm{sym}}]}_{\mathbf{r}} \\ \Rightarrow (\bar{L}_{\bar{v}}\boldsymbol{\beta}\otimes\bar{\mathbf{n}})^{sym} &= \bar{\gamma}\mathbf{m}_S - \mathbf{c}^{e-1} : \mathbf{r}\end{aligned} \tag{71}$$

and substitution of equation (69) yields:

$$(\bar{L}_{\bar{v}}\boldsymbol{\beta}\otimes\bar{\mathbf{n}})^{sym} = \dot{\bar{\alpha}}\,\mathbf{m}_S - \mathbf{c}^{e-1} : \mathbf{r} \tag{72}$$

For the frequent case in which the elastic parameters are $(\mu,\lambda) \gg \boldsymbol{\sigma}$, we can consider negligible the term $\mathbf{c}^{e-1} : \mathbf{r}$ in equations (71) and (72), which finally reads:

$$(\bar{L}_{\bar{v}}\boldsymbol{\beta}\otimes\bar{\mathbf{n}})^{sym} = \dot{\bar{\alpha}}\,\mathbf{m}_S \tag{73}$$

In addition, from equations (73) and (64) the following properties follow for the kinematic entities at the interface of discontinuity $\mathcal{S}$:

1) By equating expressions for the tensor $\mathbf{d}$ given in equations (15) ($\mathbf{d} = \mathrm{sym}(\mathbf{l}) = \bar{\mathbf{d}} + \frac{1}{h}(\bar{L}_{\bar{v}}\boldsymbol{\beta}\otimes\bar{\mathbf{n}})^{\mathrm{sym}}$) and (50) for $t > t_{SD}$(and, thus, $h \equiv k \to 0$):

$$\left.\begin{aligned}\mathbf{d} &= \bar{\mathbf{d}} + \tilde{\mathbf{d}} = \bar{\mathbf{d}} + \tfrac{1}{k}(\bar{L}_{\bar{v}}\boldsymbol{\beta}\otimes\bar{\mathbf{n}})^{\mathrm{sym}} \\ \mathbf{d} &= \mathbf{d}^e + \mathbf{d}^p = \mathbf{d}^e + \tfrac{1}{k}\bar{\gamma}\mathbf{m}_S = \mathbf{d}^e + \tfrac{1}{k}(\bar{L}_{\bar{v}}\boldsymbol{\beta}\otimes\bar{\mathbf{n}})^{\mathrm{sym}}\end{aligned}\right\} \Rightarrow \tag{74}$$

$$\begin{aligned}\mathbf{d}^e &= \bar{\mathbf{d}} \ \textit{(bounded)} \\ \mathbf{d}^p &= \tilde{\mathbf{d}} = \tfrac{1}{k}(\bar{L}_{\bar{v}}\boldsymbol{\beta}\otimes\bar{\mathbf{n}})^{\mathrm{sym}}\end{aligned} \tag{75}$$

which states that *the plastic flow* $\mathbf{d}^p$ *translates entirely into displacement jump*. This constitutes an extension to the finite deformation setting of a similar results already found for infinitesimal strains [20].

2) Condition $\boldsymbol{\beta}\cdot\bar{\mathbf{n}} = 0$ and, from equation (10) $J = \bar{J}\,\tilde{J} = \bar{J}$ leads to $\tau_S = J\boldsymbol{\sigma}_S = \bar{J}\boldsymbol{\sigma}_S$, stating (since $\bar{J}$ and $\boldsymbol{\sigma}_S$ are bounded entities) *the bounded character of the Kirchhoff stresses* τ_S (and also $\dot{\tau}_S$) *at the strong discontinuity regime*. This result, combined with the identity:

$$L^e_v\boldsymbol{\tau}_S = \underbrace{\dot{\boldsymbol{\tau}}_S}_{bounded} - \mathbf{l}^e\cdot\boldsymbol{\tau}_S - \boldsymbol{\tau}_S\cdot\mathbf{l}^{eT} = \underbrace{\mathbf{c}^e : \mathbf{d}^e}_{bounded} \Rightarrow \mathbf{l}^e = \textit{bounded} \tag{76}$$

states the bounded character of $\mathbf{l}^e$. Now, from equations (50) ($\mathbf{l} = \mathbf{l}^e + \mathbf{l}^p$) and (14)) ($\mathbf{l} = \bar{\mathbf{l}} + \frac{1}{h}(\bar{L}_{\bar{v}}\boldsymbol{\beta}\otimes\bar{\mathbf{n}})$):

$$\mathbf{l} = \underbrace{\mathbf{l}^e}_{bounded} + \mathbf{l}^p = \underbrace{\bar{\mathbf{l}}}_{bounded} + \tfrac{\mu_S}{k}(\bar{L}_{\bar{v}}\boldsymbol{\beta}\otimes\bar{\mathbf{n}}) \Rightarrow \mathbf{l}^p = \tfrac{1}{k}(\bar{L}_{\bar{v}}\boldsymbol{\beta}\otimes\bar{\mathbf{n}}) \tag{77}$$

This result, combined with equations (54) ($\mathbf{w}^p = \boldsymbol{\gamma}\,\hat{\mathbf{w}}$) and (69) ($\gamma = \frac{1}{k}\bar{\gamma}$) yields:

$$\begin{aligned}\mathbf{w}^p = \mathrm{skw}(\mathbf{l}^p) = \tfrac{1}{k}(\bar{L}_{\bar{v}}\boldsymbol{\beta}\otimes\bar{\mathbf{n}})^{\mathrm{skw}} = \gamma\hat{\mathbf{w}} = \tfrac{1}{k}\bar{\gamma}\hat{\mathbf{w}} \ \Rightarrow \\ \hat{\mathbf{w}} = \tfrac{1}{\bar{\gamma}}(\bar{L}_{\bar{v}}\boldsymbol{\beta}\otimes\bar{\mathbf{n}})^{\mathrm{skw}}\end{aligned} \tag{78}$$

providing a given structure to the (initially undetermined) spin $\mathbf{w}^p$ at the discontinuity interface S, in terms of the incremental jump $\boldsymbol{\beta}$ and the normal $\bar{\mathbf{n}}$.

3) Equation (73) is a set of six (due to the symmetry) algebraic equations. Again, in the local orthonormal basis $(\mathbf{e}_1, \mathbf{e}_2, \mathbf{e}_3)$, as depicted in figure 3, the components of equation (73) read (after considering equation (64) $\left(\bar{L}_{\bar{v}}\boldsymbol{\beta}\right)_1 = \bar{L}_{\bar{v}}\boldsymbol{\beta}\cdot\bar{\mathbf{n}} = 0$):

$$\begin{bmatrix} \left(\bar{L}_{\bar{v}}\boldsymbol{\beta}\right)_1 = 0 & \frac{1}{2}\left(\bar{L}_{\bar{v}}\boldsymbol{\beta}\right)_2 & \frac{1}{2}\left(\bar{L}_{\bar{v}}\boldsymbol{\beta}\right)_3 \\ \frac{1}{2}\left(\bar{L}_{\bar{v}}\boldsymbol{\beta}\right)_2 & 0 & 0 \\ \frac{1}{2}\left(\bar{L}_{\bar{v}}\boldsymbol{\beta}\right)_3 & 0 & 0 \end{bmatrix} = \frac{\bar{\gamma}}{\|\bar{\mathbf{n}}\|}\begin{bmatrix} m_{11} & m_{12} & m_{13} \\ m_{12} & m_{22} & m_{23} \\ m_{13} & m_{23} & m_{33} \end{bmatrix}_S \tag{79}$$

from which the following evolution of the incremental jump can be obtained:

$$\begin{aligned}\left(\bar{L}_{\bar{v}}\boldsymbol{\beta}\right)_1 &= 0\\ \left(\bar{L}_{\bar{v}}\boldsymbol{\beta}\right)_2 &= \bar{\gamma}\tfrac{1}{\|\bar{\mathbf{n}}\|}2m_{12}\\ \left(\bar{L}_{\bar{v}}\boldsymbol{\beta}\right)_3 &= \bar{\gamma}\tfrac{1}{\|\bar{\mathbf{n}}\|}2m_{13}\end{aligned} \tag{80}$$

together with the *strong discontinuity conditions* on the Kirchhoff's stress field:

$$m_{11}(\boldsymbol{\tau}_S) = m_{22}(\boldsymbol{\tau}_S) = m_{33}(\boldsymbol{\tau}_S) = m_{23}(\boldsymbol{\tau}_S) = 0 \qquad \forall t \geq t_{SD} \tag{81}$$

The definition of the flow tensor ($\mathbf{m} = \partial_{\boldsymbol{\tau}}\phi$) in equation (53-(c)) together with the strong discontinuity conditions (81) yield:

$$\left.\begin{aligned} m_{22}(\boldsymbol{\tau}_S) &= \tfrac{\partial\hat{\phi}(\boldsymbol{\tau})}{\partial\tau_{22}} = 0\\ m_{23}(\boldsymbol{\tau}_S) &= \tfrac{\partial\hat{\phi}(\boldsymbol{\tau})}{\partial\tau_{23}} = 0\\ m_{33}(\boldsymbol{\tau}_S) &= \tfrac{\partial\hat{\phi}(\boldsymbol{\tau})}{\partial\tau_{33}} = 0\end{aligned}\right\} \quad \forall t \geq t_{SD} \quad \Rightarrow$$

$$\hat{\phi}(\boldsymbol{\tau}) = \hat{\mathcal{F}}(\tau_{11,}\tau_{12,}\tau_{13}) = \hat{\mathcal{F}}(\tfrac{1}{\|\mathbf{n}\|}\mathcal{T}) = \hat{\mathcal{F}}(\tfrac{1}{\|\bar{\mathbf{n}}\|}\mathcal{T}) \;\Rightarrow \tag{82}$$

$$\begin{aligned}\bar{\mathbf{m}} \overset{def}{=} \partial_{\mathcal{T}}\hat{\mathcal{F}} &= \tfrac{1}{\|\bar{\mathbf{n}}\|}\left[\partial_{\tau_{11}}\hat{\mathcal{F}}\,, \partial_{\tau_{12}}\hat{\mathcal{F}},\, \partial_{\tau_{13}}\hat{\mathcal{F}}\right]\\ &= \tfrac{1}{\|\bar{\mathbf{n}}\|}\,[\underbrace{m_{11}}_{=0}, 2m_{12},\, 2m_{13}]^T\end{aligned}$$

where equations (11), (12) and (21) have been considered. Combining equations (80) and (82) one finally obtains:

$$\boxed{\bar{L}_{\bar{v}}\boldsymbol{\beta} = \bar{\gamma}\,\bar{\mathbf{m}}\;; \qquad \bar{\mathbf{m}} = \partial_{\mathcal{T}}\hat{\mathcal{F}}(\tfrac{1}{\|\bar{\mathbf{n}}\|}\mathcal{T})} \tag{83}$$

which constitutes a *discrete constitutive equation* for the jump $\boldsymbol{\beta}$ in terms of the nominal traction $\mathcal{T}$.

Finally, the discrete free energy concept can be also recovered here from equations (28) and (53-a):

$$\begin{aligned}\bar{\psi}(\beta,\bar{\alpha}) &= \lim_{h\equiv\mathbf{k}\to\mathbf{0}} k\,\psi(\mathbf{F},\mathbf{F}^p,\alpha) \\ &= \lim_{\mathbf{k}\to\mathbf{0}} \underbrace{k\psi^e(\mathbf{b}^e)}_{\bar{\psi}^e=0} + \lim_{\mathbf{k}\to\mathbf{0}} \underbrace{k\frac{1}{2}\mathcal{H}\alpha^2}_{\bar{\mathsf{H}}^p(\bar{\alpha})=\frac{1}{2}\bar{\mathcal{H}}\bar{\alpha}^2} = \tfrac{1}{2}\bar{\mathcal{H}}\bar{\alpha}^2 \end{aligned} \tag{84}$$

where the bounded character of $\psi^e(\mathbf{b}^e)$[12] and equations (67) and (68) have been considered. By collecting the previous results, the following discrete elastoplastic constitutive model is obtained:

Freee energy:	$\bar{\psi}(\boldsymbol{\beta},\alpha) = \underbrace{\bar{\psi}^e}_{=0} + \underbrace{\frac{1}{2}\bar{\mathcal{H}}\bar{\alpha}^2}_{\bar{H}^p(\bar{\alpha})}$	(a)
Plastic flow rule:	$\bar{L}_{\bar{v}}\boldsymbol{\beta} = \bar{\gamma}\,\bar{\mathbf{m}} \quad ; \quad \bar{\mathbf{m}} = \partial_T\hat{\mathcal{F}}(\frac{1}{\|\bar{\mathbf{n}}\|}\mathcal{T})$	(b)
Evolution law:	$\dot{\bar{\alpha}} = \bar{\gamma}$	(c)
Yield criterion:	$\mathcal{F}(\frac{1}{\|\bar{\mathbf{n}}\|}\mathcal{T}, q_S) \equiv \hat{\mathcal{F}}(\frac{1}{\|\bar{\mathbf{n}}\|}\mathcal{T}) - q_S$	(d)
Load.-unl. conditions:	$\bar{\gamma} \geq 0 \qquad \mathcal{F} \leq 0 \qquad \bar{\gamma}\,\mathcal{F} = 0$	(e)
Softening. rule:	$q_S = \partial_{\bar{\alpha}}\mathsf{H}^p(\bar{\alpha})$ $\dot{q}_S = \partial_{\bar{\alpha}\bar{\alpha}}\bar{\mathsf{H}}^p(\bar{\alpha})$ $\dot{\bar{\alpha}} = \bar{\mathcal{H}}\,\dot{\bar{\alpha}}$ $\left\{ \begin{array}{l} q_S \in [0, q_{SD}] \\ q_S\vert_{t=t_{SD}} \overset{not}{=} q_{SD} \end{array} \right.$	(f)

(85)

It is readily observed that the constitutive model (85) is *a rigid-plastic* model, since the elastic counterpart, $\bar{\psi}^e$, of the resulting discrete free energy is null. This fact can be also observed from equation (85-(b)) since unloading, characterized by $\bar{\gamma} = 0$, results in $\bar{L}_{\bar{v}}\boldsymbol{\beta} = \mathbf{0}$, and no evolution of the total displacement jump takes place as corresponds to an infinite (rigid) instantaneous

[12] The bounded character of $\mathbf{b}^e$ can be stated from the constitutive equation (53-b) ($\boldsymbol{\tau}_S = \lambda tr(Ln\sqrt{\mathbf{b}^e})\mathbb{I} + 2\mu(Ln\sqrt{\mathbf{b}^e})$) and the fact that $\boldsymbol{\tau}_S$ is a bounded entity. From that, the bounded character of the elastic free energy (53-(a)) ($\psi^e(\mathbf{b}^e) = \frac{1}{2}\lambda\ tr^2(Ln\sqrt{\mathbf{b}^e}) + \mu\ \ Ln\sqrt{\mathbf{b}^e} : Ln\sqrt{\mathbf{b}^e}$) for $t > t_{SD}$ follows trivially.

elastic stiffness. This extends to the finite strain settings the same property observed for the induced discrete plasticity models at infinitesimal strains [20].

4 CONCLUSIONS

Throughout the previous sections the strong discontinuity approach (SDA) for different constitutive models in finite strain settings has been explored. Although the topic had already been tackled in slightly different contexts [2], [12] here we have extended the results found by the authors in infinitesimal strain settings [22], [20],[23] to the large strain case. As the main result we have shown that the strong discontinuity analysis procedures used there can be extended to the large strain case, by only changing the considered strong discontinuity kinematics (7), and the same set of conclusions are achieved. That is to say: *a)* the regularization of the softening parameter (40) in the continuum (stress-strain) constitutive model induces, via de traction continuity condition (20) and the softening regularization condition (40), projected discrete (traction-displacement jump) constitutive models, (48) and (85), at the discontinuity interface (see figure 4) *b)* this fact requires a particular stress structure to be reached at the discontinuous interface, that is determined by the strong discontinuity conditions, (44) or (81) and *c)* the variable bandwidth model of section 3.2 provides a tool to automatically induce those strong discontinuity conditions and to relate them to the fracture process zone concept, classically considered in fracture mechanics [23].

In addition, those induced discrete constitutive models keep the family character of the original continuum constitutive ones (damage or elastoplasticity) and share the common feature of being rigid models (the initial stiffness is infinite). Indeed, they are analytically different from the ones obtained in infinitesimal settings [20] since the *continuum-discrete projection*, determined by the kinematics, is different.

As in the infinitesimal strains case, the initiation and propagation of the displacement discontinuity can be here determined via standard procedures supplied by the discontinuous bifurcation analysis for finite strain cases. Finally, and as the most distinguishing feature of the SDA, for practical purposes the complete analysis and simulation can be done in a continuum format, both for the continuous and discontinuous regimes, since the discrete constitutive models are automatically induced from the traction continuity

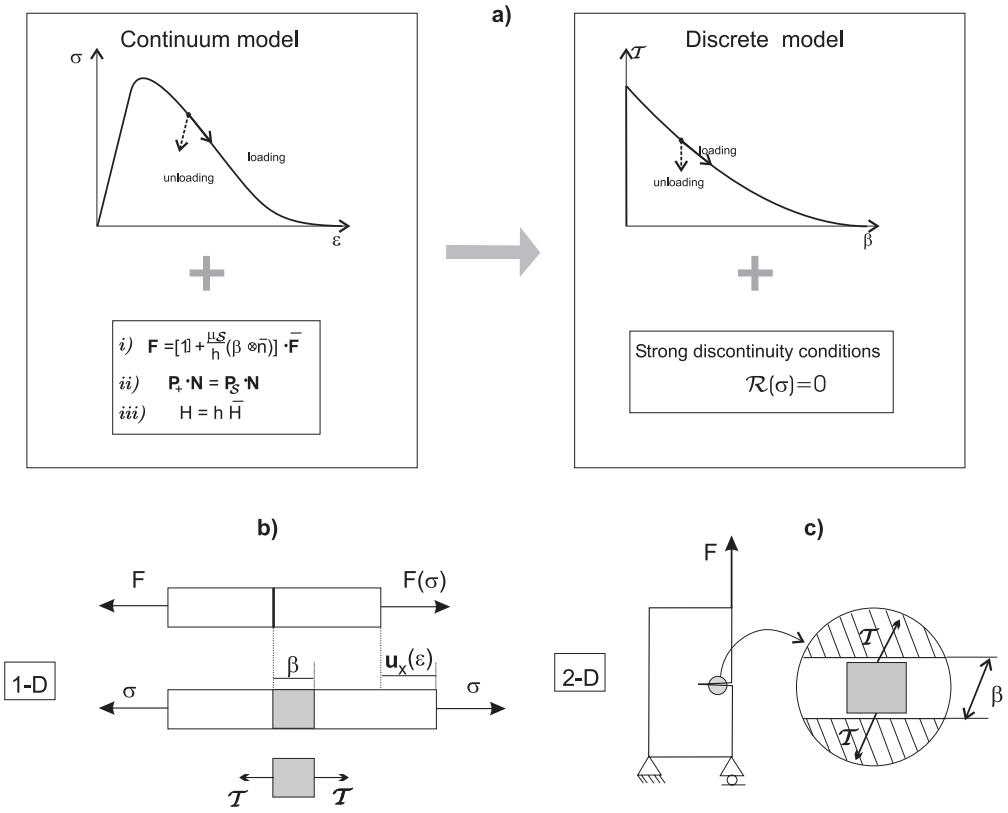

Figure 4: a) Original (continuum) versus induced (discrete) constitutive response, b) and c) induced discontinuous interfaces.

and the softening regularization. Part 2 of this work is devoted to these issues.

Acknowledgments

The second author acknowledges the Secretaria de Estado de Educación, de Universidades, Investigación y Desarrollo of Spain the financial support received through the fellowship: *Ayuda para la estancia de científicos y tecnólogos extranjeros en España*. The fourth author acknowledges the Agencia Española de Cooperación Internacional (AECI) the financial support received through the grant: *Ayudas para la realización de la Tesis Doctoral*.

APPENDIX I: Damage model, constitutive tangent tensor, localization condition, incremental integration

In this appendix additional details related to the damage constitutive model of section 3.5 are presented. First we particularize the damage function (30-e) by adopting :

$$\phi(\boldsymbol{\sigma},q) = \sqrt{\boldsymbol{\sigma}\cdot\mathbf{c}_{\phi}^{-1}\cdot\boldsymbol{\sigma}} - q \;; \quad \mathbf{c}_{\phi}^{-1} = \frac{1}{2\mu_{\phi}}\mathbf{I} - \frac{\lambda_{\phi}}{2\mu_{\phi}(2\mu_{\phi}+3\lambda_{\phi})}\,\mathbf{1}\otimes\mathbf{1} \quad \text{(AI-1)}$$

$\mathbf{I}$ being the fourth order identity tensor. The surface $\phi(\boldsymbol{\sigma},q) = 0$ defines an ellipsoid of revolution in the stress space, where parameters μ_{ϕ} and λ_{ϕ} governs the ratio among its major and minor axis.

The constitutive tangent tensor associated to this damage function is given by:

$$\bar{L}_{\bar{v}}\,\boldsymbol{\tau} = \mathbf{c}^{\tan g} : \mathbf{d} = \mathbf{c}^{\tan g} : (\boldsymbol{\nabla}_{\mathbf{x}}\dot{\mathbf{u}}) \qquad \text{(AI-2)}$$

$$\begin{aligned}
\mathbf{c}^{\tan g} &= \tfrac{q}{r}\mathbf{c}^{e} + (\tfrac{rq_{,r}-q}{r^3})\Big[\tfrac{\theta-2\kappa\,\mathrm{tr}(\bar{\boldsymbol{\tau}})}{J^2}\bar{\boldsymbol{\tau}}\otimes\bar{\boldsymbol{\tau}} + (\tfrac{\zeta\mathrm{tr}(\bar{\boldsymbol{\tau}})}{J^2} - r^2)\,\bar{\boldsymbol{\tau}}\otimes\mathbf{1} \\
&\quad + \tfrac{2\omega}{J^2}\bar{\boldsymbol{\tau}}\otimes\bar{\boldsymbol{\tau}}^2\Big] \;; \qquad \text{if} \quad \dot{r} > 0 \qquad \text{(AI-3)} \\
\mathbf{c}^{\tan g} &= \tfrac{q}{r}\mathbf{c}^{e} \;; \qquad \text{if} \quad \dot{r} \le 0
\end{aligned}$$

where $\bar{\boldsymbol{\tau}} = \frac{r}{q}\boldsymbol{\tau} = (1-d)\boldsymbol{\tau}$ is the effective Kirchhoff stress**,** and $\mathbf{c}^{e}$ is the hyperelastic constitutive tensor:

$$\begin{aligned}
\mathbf{c}^{e} &= \lambda^{*}(\mathbf{1}\otimes\mathbf{1}) + 2\mu^{*}\mathbf{I} \;; \\
\lambda^{*} &= \lambda J^2 \;; \qquad \mu^{*} = \mu + \tfrac{\lambda}{2}(1-J^2)
\end{aligned} \qquad \text{(AI-4)}$$

where λ, μ are the Lame's parameters of the hyperelastic law (equation 30-a); and the scalar factors ζ, θ are :

$$\begin{aligned} \zeta = \lambda^*\omega - 3\kappa\lambda^* - 2\mu^*\kappa \; ; \qquad \theta = 2\mu^*\omega \\ \omega = \tfrac{1}{2\mu_\phi} \; ; \qquad \kappa = \tfrac{\lambda_\phi}{2\mu_\phi(2\mu_\phi+3\lambda_\phi)} \end{aligned} \tag{AI-5}$$

We write the localization tensor $\mathbf{Q}_{t_B}$ of Section 3.3 as follows :

$$\mathbf{Q}_{t_B} \overset{not}{=} \mathbf{Q}^d = \frac{q}{r}\mathbf{Q}^e \left(\mathbf{1} + \left[\frac{q_{,r}}{rq} - \frac{1}{r^2} \right] \boldsymbol{\xi} \otimes \boldsymbol{\rho} \right) \tag{AI-6}$$

$\mathbf{Q}^e = \mathbf{e}_n \cdot \mathbf{c}^e \cdot \mathbf{e}_n + (\mathbf{e}_n \cdot \bar{\boldsymbol{\tau}} \cdot \mathbf{e}_n)\,\mathbf{1}$ being the acoustic elastic tensor satisfying $\det(\mathbf{Q}^e) > 0$, and vectors $\boldsymbol{\xi}$, $\boldsymbol{\rho}$ being given by:

$$\begin{aligned} \boldsymbol{\xi} &= (\mathbf{Q}^e)^{-1} \cdot \boldsymbol{\tau} \cdot \mathbf{e}_n \\ \boldsymbol{\rho} &= \tfrac{\theta - 2\kappa\,\mathrm{tr}(\bar{\boldsymbol{\tau}})}{J^2}\boldsymbol{\tau} \cdot \mathbf{e}_n + (\tfrac{\zeta \mathrm{tr}(\boldsymbol{\tau})}{J^2} - qr)\mathbf{e}_n + \tfrac{2\omega}{J^2}\bar{\boldsymbol{\tau}}^2 \cdot \mathbf{e}_n \end{aligned} \tag{AI-7}$$

Recalling the term $q_{,r} = \mathcal{H}$, the critical softening modulus $\mathcal{H}^{crit}$ which makes singular the localization tensor $\mathbf{Q}^d$ ($\det(\mathbf{Q}^d) = 0$), is then determined through the following expression :

$$\mathcal{H}^{crit} = \frac{q}{r}\left(1 - \frac{r^2}{\boldsymbol{\xi} \cdot \boldsymbol{\rho}}\right) \tag{AI-8}$$

Damage integration algorithm

The following box describes the integration algorithm.

Box 1: Damage integration algorithm

Assume that incremental displacement are given at time $t+\Delta t$.
Then: **evaluate** the following terms

i) $\mathbf{F}_{t+\Delta t}$; $\mathbf{b}_{t+\Delta t}$; $J_{t+\Delta t}$

ii) $\bar{\boldsymbol{\tau}}_{t+\Delta t} = \lambda \frac{(J_{t+\Delta t}^2 - 1)}{2} \mathbf{1} + \mu (\mathbf{b}_{t+\Delta t} - \mathbf{1})$

iii) $\phi_{t+\Delta t}^{\text{trial}} = \frac{1}{J_{t+\Delta t}} \frac{q_t}{r_t} \sqrt{\bar{\boldsymbol{\tau}}_{t+\Delta t} \cdot \mathbf{c}_\phi^{-1} \cdot \bar{\boldsymbol{\tau}}_{t+\Delta t}} - q_t$

if $\phi_{t+\Delta t}^{\text{trial}} \leq 0$ **then**

there was *unloading* and the result of the integration step is:
$\boldsymbol{\tau}_{t+\Delta t} = \frac{q_t}{r_t} \bar{\boldsymbol{\tau}}_{t+\Delta t}$; $r_{t+\Delta t} = r_t$; $q_{t+\Delta t} = q_t$

else if $\phi_{t+\Delta t}^{\text{trial}} > 0$ **then**

there was *loading* and from the equation $\phi_{t+\Delta t} = 0$ it is obtained
$r_{t+\Delta t} = \frac{1}{J_{t+\Delta t}} \sqrt{\bar{\boldsymbol{\tau}}_{t+\Delta t} \cdot \mathbf{c}_\phi^{-1} \cdot \bar{\boldsymbol{\tau}}_{t+\Delta t}}$
which finally determines:
$q_{t+\Delta t} = q_t + \mathcal{H}(r_{t+\Delta t} - r_t)$; $\boldsymbol{\tau}_{t+\Delta t} = \frac{q_{t+\Delta t}}{r_{t+\Delta t}} \bar{\boldsymbol{\tau}}_{t+\Delta t}$

endif

This algorithm is slightly modified in the weak discontinuity regime to take into account the bandwidth variation, and hence the softening modulus dependence with q.

APPENDIX II: Additional topics on the elasto-plastic model and the integration algorithm

The following hypotheses of the elastoplastic model have been considered:

- The elastic response is isotropic: the elastic left Cauchy-Green deformation tensor $\mathbf{b}^e = \mathbf{F}^e \cdot \mathbf{F}^{eT}$ is colinear with $\boldsymbol{\tau}$. Let $\mathbf{g}_i$ and $(\lambda_i^e)^2$ $(i = 1, 2, 3)$ be the eigenvectors and principal values of $\mathbf{b}^e$ ($\mathbf{b}^e = (\lambda_i^e)^2 \mathbf{g}_i \otimes \mathbf{g}_i$). Then, $\boldsymbol{\tau}$ has the same eigenvectors ($\boldsymbol{\tau} = \tau_i \mathbf{g}_i \otimes \mathbf{g}_i$, with τ_i the principal values of the Kirchhoff stress).

- Plastic isotropy: the yield function $\phi(\boldsymbol{\tau}, q)$ is an isotropic function of $\boldsymbol{\tau}$ and $\partial_{\boldsymbol{\tau}} \phi$ is colinear with $\boldsymbol{\tau}$. The internal variable q and its dual variable α, related to the isotropic hardening mechanism, are scalars.

By using the principal values of $\boldsymbol{\tau}$ and $\mathbf{b}^e$, equation (53-b) can be rewritten as :

$$\tau_i = \lambda(\varepsilon_1^e + \varepsilon_2^e + \varepsilon_3^e) + 2\mu\varepsilon_i^e \tag{AII-1}$$

where $\varepsilon_i^e = \ln \lambda_i^e$. The elastic constitutive tensor $\mathbf{c}^e$ results (see [6], page 90):

$$\mathbf{c}^e = c_{ijkl}^e \left(\mathbf{g}_i \otimes \mathbf{g}_j \otimes \mathbf{g}_k \otimes \mathbf{g}_l\right) \tag{AII-2}$$

with components c_{ijkl}^e given by:

$$\begin{aligned} c_{iijj}^e &= \lambda + 2(\mu - \tau_i)\delta_{ij} \\ c_{ijij}^e &= c_{ijji}^e = c_{jiij}^e = \frac{\lambda_j^{e\,2}\tau_i - \lambda_i^{e\,2}\tau_j}{\lambda_i^{e\,2} - \lambda_j^{e\,2}} \qquad (i \neq j) \end{aligned} \tag{AII-3}$$

These expressions are meaningful if the principal stretches are unequal ($\lambda_i^e \neq \lambda_j^e$). Otherwise the reader is referred to reference [6].

Next, we sketch the integration algorithm used in the numerical applications. We follow the work of Simo ([30], [28]). This author considered the assumption $\mathbf{w}^p = \mathbf{0}$ (which is not strictly verified by the integration scheme proposed in that work). Nevertheless, from the fact that the plastic spin in the relaxed configuration $(\mathbf{L}^p)^{\text{skw}}$ is arbitrary (it does not need to be constitutively defined in an isotropic elasto-plastic model with scalar internal variables[13] ([7])), it relieves the inconsistency of this assumption respect to the considerations adopted in this paper.

[13] Alternatively, this statement can also be rephrased in terms of the intermediate plastic configuration associated to the multiplicative decomposition (49). As a mater of fact, for isotropic elastoplastic models with scalar internal variables, that intermediate configuration is defined by the constitutive model (53) *except for a rotation which remains undetermined*.

Using the flow law (53-c), one can write :

$$\mathbf{F}^e \cdot \mathbf{L}^p \cdot \mathbf{F}^{e\,-1} = \gamma \mathbf{m} \tag{AII-4}$$

From the polar decomposition $\mathbf{F}^e = \mathbf{V}^e \cdot \mathbf{R}^e$, recalling the colinearity of tensors $\mathbf{m}$ and $\mathbf{V}^e$, we obtain from (AII-4) :

$$\mathbf{L}^p = \gamma \mathbf{R}^{eT} \cdot \mathbf{m} \cdot \mathbf{R}^e \tag{AII-5}$$

We use an exponential approximation to integrate $\dot{\mathbf{F}}^p = \mathbf{L}^p \cdot \mathbf{F}^p$ from time t to time $t + \Delta t$, resulting :

$$\mathbf{F}^p{}_{t+\Delta t} = \exp(\Delta t \mathbf{L}^p_{t+\Delta t}) \cdot \mathbf{F}^p{}_t \tag{AII-6}$$

Taking into account that $\mathbf{F}_{t+\Delta t} = \mathbf{F}^e{}_{t+\Delta t} \cdot \mathbf{F}^p{}_{t+\Delta t}$, equation(AII-6) can be rearranged to give :

$$\mathbf{F}^e{}_{t+\Delta t} = (\mathbf{F}^e)^{\text{trial}} \cdot \exp(-\Delta t \mathbf{L}^p_{t+\Delta t}) \tag{AII-7}$$

where we call $(\mathbf{F}^e)^{\text{trial}} = \mathbf{F}_{t+\Delta t} \cdot (\mathbf{F}^p{}_t)^{-1}$. Equation (AII-7) can be put alternatively as:

$$\mathbf{V}^e{}_{t+\Delta t} = (\mathbf{V}^e)^{\text{trial}} \cdot \exp(-\Delta \gamma \mathbf{m}_{t+\Delta t}) \tag{AII-8}$$

where $\Delta\gamma = \gamma \Delta t$ and $\mathbf{R}^e{}_{t+\Delta t} = (\mathbf{R}^e)^{\text{trial}}$; or by using the principal values of each tensor

$$(\lambda^e_{t+\Delta t})_i = (\lambda^e)^{\text{trial}}_i \exp(-\Delta\gamma \; m_{it+\Delta t}) \; , \qquad i = 1,2,3 \tag{AII-9}$$

which results :

$$\begin{aligned} (\varepsilon^e_i)_{t+\Delta t} &= (\ln \lambda^e_{t+\Delta t})_i = (\ln \lambda^{\text{trial}}_e)_i - \Delta t \; m_{it+\Delta t} \\ &= (\varepsilon^e)^{\text{trial}}_i - \Delta\gamma \, m_{it+\Delta t} \; , \qquad i = 1,2,3 \end{aligned} \tag{AII-10}$$

Finally, given $\mathbf{F}_{t+\Delta t}$ and $(\mathbf{F}^e)^{\text{trial}}$, equations (AII-10), (53-g) in incremental form:

$$q_{t+\Delta t} = q_t + \mathcal{H} \Delta\gamma \tag{AII-11}$$

and (AII-1):

$$\tau_{it+\Delta t} = \lambda(\varepsilon^e_{1\,t+\Delta t} + \varepsilon^e_{2\,t+\Delta t} + \varepsilon^e_{3\,t+\Delta t}) + 2\mu(\varepsilon^e_{i\,t+\Delta t}) \qquad \text{(AII-12)}$$

plus the loading-unloading conditions (53-f) which we rewrite in incremental form :

$$\Delta\gamma \geq 0 \qquad \phi(\boldsymbol{\tau}_{t+\Delta t}, q_{t+\Delta t}) \leq 0 \qquad \Delta\gamma\,\phi(\boldsymbol{\tau}_{t+\Delta t}, q_{t+\Delta t}) = 0 \qquad \text{(AII-13)}$$

determine all unknowns ($\tau_{it+\Delta t}$, $q_{t+\Delta t}$, $\Delta\gamma$, $\mathbf{F}^p{}_{t+\Delta t}$ and $\mathbf{F}^e{}_{t+\Delta t}$) in the loading step. This equation set can be solved in the same way as it is done in the infinitesimal model, i.e. by using a return mapping algorithm.

The algorithmic tangent tensor for this integration procedure, $\mathcal{C}^{\text{algor}}_{t+\Delta t}$, is defined through:

$$\bar{L}_{\bar{v}}\,\boldsymbol{\tau}_{\,t+\Delta t} = \mathcal{C}^{\text{algor}}_{t+\Delta t} : \mathbf{d}_{t+\Delta t} = \mathcal{C}^{\text{algor}}_{t+\Delta t} : (\boldsymbol{\nabla}^S_{\mathbf{x}}\dot{\mathbf{u}}_{t+\Delta t}) \qquad \text{(AII-14)}$$

Further details on the structure of $\mathcal{C}^{\text{algor}}_{t+\Delta t}$ for this particular model can be found in the work of Simo [30].

References

[1] F. Armero. Localized anisotropic damage of brittle materials. In D.R.J. Owen, E. Onate, and E. Hinton, editors, *Computational Plasticity. Fundamentals and Applications*, pages 635–640, 1997.

[2] F. Armero and K. Garikipati. An analysis of strong discontinuities in multiplicative finite strain plasticity and their relation with the numerical simulation of strain localization in solids. *Int.J. Solids and Structures*, 33(20–22):2863–2885, 1996.

[3] T. Belytschko, N. Moes, S. Usui, and C. Parimi. Arbitrary discontinuities in finite elements. *Int. J. Numer. Meth. Engng.*, (50):993–1013, 2001.

[4] D. Bigoni and D Zaccaria. On strain localization analysis of elastoplastic materials at finite strains. *Int.J.of Plasticity*, 9:21–33, 1993.

[5] R. De Borst, L.J. Sluys, H.B. Mulhaus, and J. Pamin. Fundamental issues in finite element analyses of localization of deformation. *Eng. Computation*, 10:99–121, 1993.

[6] M. A. Crisfield. *Non-linear Finite Element Analysis of Solids and Structures, Volume 2: Advanced Topics*. John Wiley & Sons, 1998.

[7] Y. F. Dafalias. Common misunderstanding in finite deformation anisotropic plasticity. In E. Hinton D.R.J. Owen, E. Onate, editor, *Computational Plasticity, Fundamentals and Appl.*, pages 367–378. Cimne, Barcelona, 1997.

[8] E.N. Dvorkin, A.M. Cuitino, and G. Gioia. Finite elements with displacement embedded localization lines insensitive to mesh size and distortions. *International journal for numerical methods in engineering*, 30:541–564, 1990.

[9] K. Garikipati and T.J.R. Hughes. A study of strain-localization in a multiple scale framework. The one dimensional problem. *Comput. Methods Appl. Mech. Engrg. (to appear)*, 1996.

[10] M. Jirasek. Finite elements with embedded cracks. *Internal Report - Ecole Polytechnique Federale de Lausanne*, LSC Internal Report 98/01, April 1998.

[11] R. Larsson, K. Runesson, and S. Sture. Embedded localization band in undrained soil based on regularized strong discontinuity theory and finite element analysis. *Int.J. Solids and Structures*, 33(20–22):3081–3101, 1996.

[12] R. Larsson, P. Steinmann, and K. Runesson. Finite element embedded localization band for finite strain plasticity based on a regularized strong discontinuity. *Mechanics of Cohesive Frictional Materials*, 4:171–194, 1998.

[13] H.R. Lofti and P.Benson Ching. Embedded representation of fracture in concrete with mixed finite elements. *International journal for numerical methods in engineering*, 38:1307–1325, 1995.

[14] J. Lubliner. *Plasticity Theory*. Mcmillan Publishing Company, 1990.

[15] A. Molinari and R.J. Clifton. Analytical characterization of shear localization in thermoviscoplastic materials. *J. of Applied Mechanics*, 54(December):806–812, 1987.

[16] J. Oliver. Continuum modelling of strong discontinuities in solid mechanics using damage models. *Computational Mechanics*, 17(1–2):49–61, 1995.

[17] J. Oliver. Modeling strong discontinuities in solid mechanics via strain softening constitutive equations. Part 1: Fundamentals. *Int.J.Num.Meth.Eng.*, 39(21):3575–3600, 1996.

[18] J. Oliver. Modeling strong discontinuities in solid mechanics via strain softening constitutive equations. Part 2: Numerical simulation. *Int.J.Num.Meth.Eng.*, 39(21):3601–3623, 1996.

[19] J. Oliver. The strong discontinuity approach: an overview. In Idelsohn S., Oñate E., and Dvorkin E.N., editors, *Computational Mechanics. New Trends and Applications. (WCCM98) Proceedings (CD-ROM) of the IV World Congress on Computational Mechanics*, Barcelona, 1998. CIMNE.

[20] J. Oliver. On the discrete constitutive models induced by strong discontinuity kinematics and continuum constitutive equations. *International Journal Solids and Structures*, 37:7207–7229, 2000.

[21] J. Oliver, M. Cervera, and O. Manzoli. On the use of J2 plasticity models for the simulation of 2D strong discontinuities in solids. In D.R.J. Owen, E. Onate, and E. Hinton, editors, *Proc. Int. Conf. on Computational Plasticity*, pages 38–55, Barcelona (Spain), 1997. C.I.M.N.E.

[22] J. Oliver, M. Cervera, and O. Manzoli. Strong discontinuities and continuum plasticity models: The strong discontinuity approach. *International Journal of Plasticity*, 15(3):319–351, 1999.

[23] J. Oliver, A. Huespe, M.D.G. Pulido, and E. Chaves. From continuum mechanics to fracture mechanics: the strong discontinuity approach. *Engineering Fracture Mechanics*, (in press), 2001.

[24] J. Planas, M. Elices, and G.V. Guinea. Cohesive cracks versus nonlocal models: Closing the gap. *International Journal of Fracture*, (63):173–187, 1993.

[25] R. Regueiro and R. I. Borja. A finite element model of localized deformation in frictional materials taking a strong discontinuity approach. *Finite Elements in Analysis and Design*, 33:283–315, 1999.

[26] J. Rice. The localization of plastic deformation. In *Theoretical and Applied Mechanics*, pages 207–219. North-Holland Publ. Co., 1976.

[27] J. Simo. *Numerical Analysis of Classical Plasticity*, volume IV of *Handbook for Numerical Analysis* edited by P.G. Ciarlet and J.J. Lions . in press.

[28] J. Simo. *Numerical Analysis of Classical Plasticity*, volume IV of *Handbook for Numerical Analysis* edited by P.G. Ciarlet and J.J. Lions . Elsevier Sc. Publisher (North-Holland).

[29] J. Simo and J. Oliver. A new approach to the analysis and simulation of strong discontinuities. In Z.P. Bazant et al., editor, *Fracture and Damage in Quasi-brittle Structures*, pages 25–39, 1994. E & FN Spon.

[30] J.C. Simo. Algorithm for static and dynamic multiplicative plasticity that preserve the calssical return mapping schemes of the infinitesima theory. *Comp. Meth. Appl. Mech. Eng.*, 99:61–112, 1992.

[31] J.C. Simo and T.J.R. Hughes. *Computational Inelasticity*. Springer, 1998.

[32] V. Tvergaard. Studies of elastic-plastic instabilities. *J. of Applied Mechanics*, 66(March):3–9, 1999.

[33] I. Vardoulakis. Stability and bifurcation in geomechanics: strain localization in granular materials. In *Lecture Notes, Univ. Politecnica de Catalunya*, October, 1999.

[34] G.N. Wells and L.J. Sluys. Application of continuum laws in discontinuity analysis based on a regularized displacement discontinuity. In *ECCM'99, Eur. Conf. on Comp. Mech.*, Aug.31-Sept.3 1999.

[35] K. Willam. *Constitutive models for materials, in: Encyclopedia of Physical Science & Technology , 3rd edition*. Academic Press, 2000.

On the strong discontinuity approach in finite deformation settings. Part 2: Numerical simulation.

Abstract

This second part of the work is devoted to developing the large strain counterpart of the nonsymmetric finite element with embedded discontinuity, frequently considered in the Strong Discontinuity Approach, and to performing numerical experiments to display the theoretical aspects tackled in Part 1 of this work, as well as to emphasizing the role of the large strain kinematics in the obtained results.

keywords: Strong discontinuity approach, damage models, elastoplastic models

1 INTRODUCTION

In Part I of this work [15] the theoretical aspects of the strong discontinuity approach (SDA) at large strains have been presented. The main result in there is that, on the basis of any standard (stress-strain) continuum constitutive model [1] and introducing the following ingredients:

- large-strain strong discontinuity kinematics
- regularization of the softening law

[1] As a matter of example, in Part 1 isotropic elasto-plastic and continuum damage models have been considered as *target* models, but the obtained conclusions are not restricted to those particular constitutive models.

- nominal traction continuity across the discontinuous interface,

a discrete (traction-displacement jump) constitutive model is naturally induced at the discontinuity interface, as a 2D projection of the original 3D constitutive law. The directionality of such projection is provided by the normal to the interface which, in turn, is obtained from the classical discontinuous bifurcation analysis [21],[16].

Consequently, the main feature of the SDA is that both the bulk of the body and the discontinuity interface can be treated in a *continuum format* using the *same* continuum constitutive model. Therefore, unlike the classical *discrete* approaches, the SDA does not require the explicit introduction of *ad hoc* discrete decohesive constitutive equations at the interface of discontinuity, since it is automatically induced by the kinematics which, in turn, is consistent with the phenomenological motivations of the continuum model. In addition, some typical numerical difficulties found in the discrete approaches[2] are naturally overcome in the SDA.

This Part2 of the work is devoted to the numerical aspects of the SDA, essentially to: 1) describe the ingredients required for the numerical simulation of solid mechanics problems involving strong discontinuities and 2) perform numerical experiments in order to confirm and highlight the theoretical results obtained in Part 1. For the sake of simplicity only 2D problems shall be considered here, leaving the 3D case for future works.

For numerical simulation purposes, the SDA requires its particular kinematics to be captured by the selected numerical procedure. In the context of the finite element method, this suggests the use of the so called *finite elements with embedded discontinuities* [6],[10],[18],[12],[2]. In reference [8] one can find a review of the different approaches proposed in the technical literature on the subject. The topic is not closed at all and intensive research is currently undertaken aiming at developing more robust and reliable finite elements to capture strong discontinuities. [5],[4], [7],[17],[20].

The remaining of this paper is structured as follows: in section 2 a description of the finite element technology, for the large strain kinematics case, is provided. Section 3 is devoted to present a set of numerical simulations in

[2]For instance, the numerical difficulties found to match the *rigid* behaviour required to provide physical meaning to the discrete constitutive equation. This is commonly approached by means of elastic-plastic, or elastic-damage, decompositions of the displacement-jump field, combined with a numerical penalization of the elastic counterpart that is a source of ill-conditioning problems.

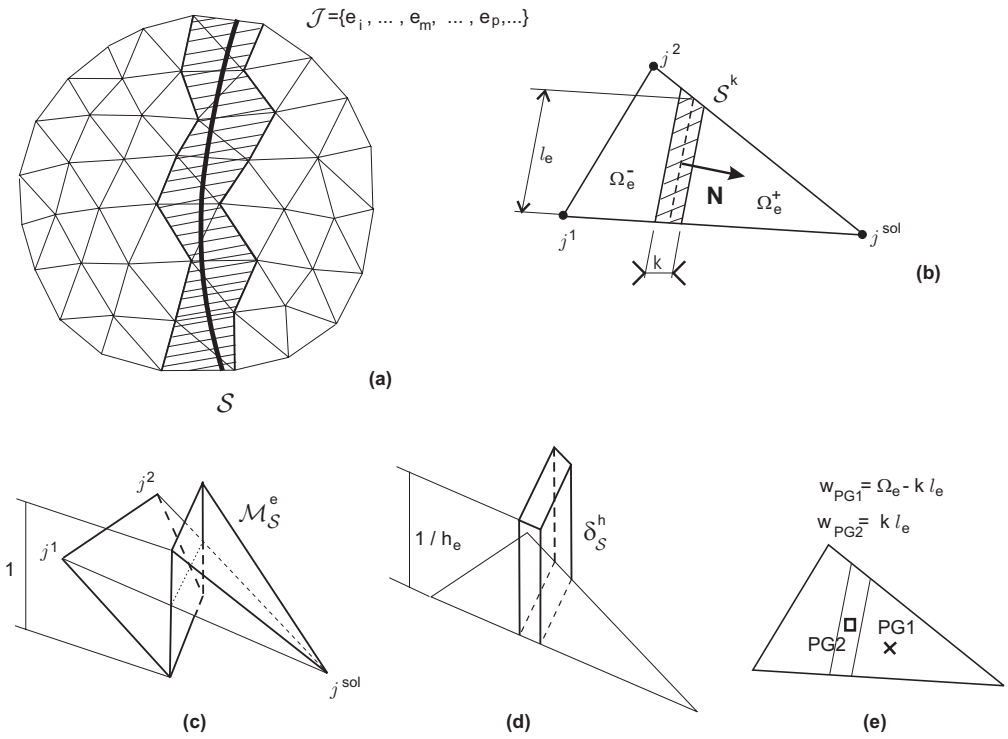

Figure 1: Finite element with embedded discontinuity

the context of the SDA, for both of the families of constitutive models tackled in Part 1 i.e.: continuum damage models and plasticity models. Finally some concluding remarks are presented.

2 FINITE ELEMENT APPROACH

Conceptually there are not substantial differences between the finite element technology for the infinitesimal strain case, reported elsewhere [12], and the one used here for the numerical simulations in large strain settings. Therefore, in this section only a brief sketch of the considered finite element with embedded discontinuity will we provided, emphasizing the specific features introduced by the large deformation kinematics.

2.1 Discretized displacement field

Let us consider the material domain Ω discretized in a triangular[3] finite element mesh with n_{elem} elements and n_{node} nodes crossed by the discontinuity interface $\mathcal{S}$(see figure 1a). Let us then consider the subset $\mathcal{J}$ of the $n_{\mathcal{J}}$ elements that are crossed by $\mathcal{S}$ at the considered time t :

$$\mathcal{J} \equiv \{e \mid \Omega_e \cap \mathcal{S} \neq \emptyset\} = \{e_{i,}....,e_{m,}....e_p,...\} \tag{1}$$

This subset is determined by means of an specific algorithm devoted to track the discontinuity [12]. For every element of $\mathcal{J}$, the *tracking algorithm* also provides the position of the elemental discontinuity interface $\mathcal{S}_e$ (see figure 1b) of length l_e which defines the domains Ω_e^+ and Ω_e^- and leaves one node at one side of the element (the *solitary node* j^{sol}) and two nodes ($j^1$and j^2) at the other side. The sense of the normal $\mathbf{N}$ inside the element is chosen to point toward the solitary node side Ω_e^+.

Based on this, and motivated by the kinematics presented in Part 1 of this work, we consider the following interpolation of the (rate of) displacement field $\mathbf{u}^{(e)}$inside a given element e [12]:

$$\dot{\mathbf{u}}^{(e)}(\mathbf{X},t) = \dot{\bar{\mathbf{u}}}^{(e)} + \dot{\tilde{\mathbf{u}}}^{(e)} = \underbrace{\Sigma_{i=1}^{i=3}\, N_i^{(e)}(\mathbf{X})\dot{\mathbf{d}}_i(t)}_{\dot{\bar{\mathbf{u}}}^{(e)}} + \underbrace{\mathcal{M}_{\mathcal{S}}^{(e)}(\mathbf{X})\,[[\dot{\mathbf{u}}]]_e(t)}_{\dot{\tilde{\mathbf{u}}}^{(e)}} \tag{2}$$

where $\dot{\bar{\mathbf{u}}}^{(e)}$ is the standard $\mathcal{C}^0$displacement field, interpolated by the shape functions $\{N_1^{(e)}, N_2^{(e)}, N_3^{(e)}\}$ of the linear isoparametric triangle [22], in terms of the nodal displacements $\mathbf{d}_i(t)$ at node i. The term $\dot{\tilde{\mathbf{u}}}^{(e)}$, in equation (2), captures the singular (discontinuous) part of the displacement field in terms of the *elemental displacement jump* $[[\dot{\mathbf{u}}]]_e$ and the *unit jump function* $\mathcal{M}_{\mathcal{S}}^e(\mathbf{X})$ defined as follows:

$$\mathcal{M}_{\mathcal{S}}^{(e)}(\mathbf{X}) = \begin{cases} 0 \quad \forall\, e \notin \mathcal{J} \\ \mathcal{H}_{\mathcal{S}}^{(e)}(\mathbf{X}) - N_{sol}^{(e)}(\mathbf{X}) \quad \forall\, e \in \mathcal{J} \end{cases} \tag{3}$$

[3]From now on the three noded (constant stress) triangle will be considered as the *basic* element for explanation purposes. Generalization to other families of finite elements can also be done but it is out of the scope of this work.

where $\mathcal{H}_{\mathcal{S}}^{(e)}$ is the step function ($\mathcal{H}_{\mathcal{S}}^{(e)}(\mathbf{X}) = 1 \ \forall \mathbf{X} \in \Omega_e^+$ and $\mathcal{H}_{\mathcal{S}}^{(e)}(\mathbf{X}) = 0 \ \forall \mathbf{X} \in \Omega_e^-$) and the index "*sol*" refers to the solitary node. Figure 1c shows the $\mathcal{M}_{\mathcal{S}}^{(e)}$ function and emphasizes its elemental support.

The term $\mathcal{M}_{\mathcal{S}}^{(e)}(\mathbf{X})\,[[\dot{\mathbf{u}}]]_e(t)$ in equation (2) can be regarded as an enhancement of the basic displacement field $\Sigma_{i=1}^{i=3} N_i^{(e)}(\mathbf{X})\dot{\mathbf{d}}_i(t)$, provided by the underlying isoparametric finite element, which due to the particular structure of the *unit jump function* $\mathcal{M}_{\mathcal{S}}^{e}$ in equation (3) makes the resulting displacement field discontinuous.

The kinematics of equation (2) can be also expressed in compact form as:

$$\begin{aligned} \dot{\mathbf{u}}(\mathbf{X},t) &= \bar{\mathbf{N}}(\mathbf{X}) \cdot \dot{\mathbf{d}}(\mathbf{t}) \ + \tilde{\mathbf{M}}(\mathbf{x}) \cdot \dot{\boldsymbol{\gamma}}(\mathbf{t}) \\ \dot{\mathbf{d}} \equiv \left\{ \dot{\mathbf{d}}_{1,}....,\dot{\mathbf{d}}_{n_{node}} \right\}^T \ ; \quad \dot{\boldsymbol{\gamma}} &\equiv \left\{ [[\dot{\mathbf{u}}]]_1, ..., [[\dot{\mathbf{u}}]]_{n_{\mathcal{J}}} \right\}^T \end{aligned} \tag{4}$$

From equations (2) and (3), the discrete (rate of) deformation gradient reads:

$$\begin{aligned} \dot{\mathbf{F}}^{(e)} \overset{def}{=} \dot{\mathbf{u}}^{(e)} \otimes \nabla_{\mathbf{X}} \ = \ & \underbrace{\Sigma_{i=1}^{i=3} \left(\dot{\mathbf{d}}_i \otimes \nabla_{\mathbf{X}} N_i^{(e)} \right) - \left([[\dot{\mathbf{u}}]]_e \otimes \nabla_{\mathbf{X}} N_{sol}^{(e)} \right)}_{\dot{\bar{\mathbf{F}}}^{(e)} \ (bounded)} \\ & + \delta_{\mathcal{S}} \left([[\dot{\mathbf{u}}]]_e \otimes \mathbf{N} \right) \end{aligned} \tag{5}$$

where $\delta_{\mathcal{S}}$ stands for Dirac's delta function emerging from the spatial derivation of the Heaviside function $\mathcal{H}_{\mathcal{S}}^{(e)}$ in equation (3) ($\nabla_{\mathbf{X}} \mathcal{H}_{\mathcal{S}}^{(e)}(\mathbf{X}) = \delta_{\mathcal{S}} \mathbf{N}$). Notice that equation (5) exactly matches the strong discontinuity kinematics discussed in Part 1.

As pointed out there, in order to overcome the numerical difficulties of treating with the Dirac's delta function, and also to model the transition from the weak to the strong discontinuity regimes, $\delta_{\mathcal{S}}$ is replaced by a regularized function $\delta_{\mathcal{S}}^e$ defined within the element e as:

$$\delta_{\mathcal{S}}^{(e)} = \mu_{\mathcal{S}}^{(e)} \frac{1}{h_e} \tag{6}$$

where h_e is the *elemental bandwidth,* defined according the variable bandwidth model outlined in Part 1, and $\mu_{\mathcal{S}}^{(e)}$ is a collocation function whose support is the domain $\mathcal{S}_e^k$ in figure 1b defined in terms of the regularization parameter k :

$$\begin{aligned} \mu_{\mathcal{S}}^{(e)}(\mathbf{X}) &= 1 \quad \forall\ \mathbf{X} \in \mathcal{S}_e^k \\ \mu_{\mathcal{S}}^{(e)}(\mathbf{X}) &= 0 \quad \forall\ \mathbf{X} \notin \mathcal{S}_e^k \end{aligned} \tag{7}$$

By considering equations (6) and (7) the regularized form of the rate of deformation gradient (5) reads:

$$\dot{\mathbf{F}}^{(e)} = \underbrace{\Sigma_{i=1}^{i=3}\ (\dot{\mathbf{d}}_i \otimes \nabla_{\mathbf{X}} N_i^{(e)}) - ([[\dot{\mathbf{u}}]]_e \otimes \nabla_{\mathbf{X}} N_{sol}^{(e)})}_{\dot{\bar{\mathbf{F}}}^{(e)}\ \text{(bounded)}} + \underbrace{\mu_{\mathcal{S}}^{(e)} \frac{1}{h_e}([[\dot{\mathbf{u}}]]_e \otimes \mathbf{N})}_{\text{unbounded for } h_e \to 0} \tag{8}$$

In order to integrate the discontinuous terms emerging from the second term of the right-hand-side of equation (8), in addition to the regular sampling point of the constant strain triangle (PG1 in figure 1e), the element is equipped with a second integration point (PG2 in figure 1e) whose associated area is:

$$meas\,(S_e^k) = kl_e \tag{9}$$

The regularization parameter k has an arbitrary small value (as small as permitted by the machine precision). Therefore, integration of regular (bounded) terms in $\mathcal{S}_e^k$ results in arbitrary small values, which makes the approach consistent. Also notice that neither k nor h_e are associated to any length of the finite element or mesh.

2.2 Body equilibrium and discrete equilibrium equations

Let us consider the material configuration of the solid, Ω, with boundary $\partial\Omega = \Gamma_u \cup \Gamma_\sigma$, where Γ_u is the part of that boundary where displacements are prescribed and Γ_σ the one were tractions are given(see figure 2), crossed by the discontinuity interface S that splits Ω into the domains Ω^+ and Ω^-. The local equilibrium of the body is described by the following equations:

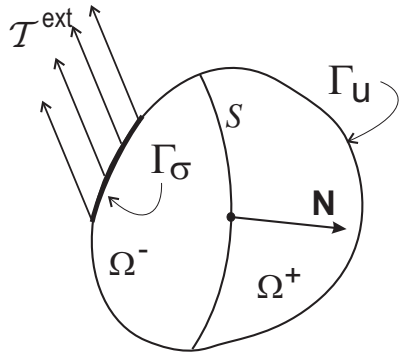

Figure 2: Strong discontinuity in a body

$$\begin{aligned} &\underbrace{\mathbf{P}\cdot\boldsymbol{\nabla}_{\mathbf{X}}}\ +\boldsymbol{\rho}_0\bar{\mathbf{B}}=\mathbf{0} \quad \text{for} \quad (\mathbf{X},t)\in\Omega\backslash S\times[0,T] \\ &\overset{not}{=} DIV\,(P) \\ &\mathbf{P}\cdot\mathbf{N}=\mathcal{T}^{\text{ ext}} \qquad\quad \text{for} \quad (\mathbf{X},t)\in\Gamma_\sigma\times[0,T] \\ &\mathbf{P}_{\Omega^+}\cdot\mathbf{N}=\mathbf{P}_{\Omega^-}\cdot\mathbf{N} \quad \text{for} \quad (\mathbf{X},t)\in S\times[0,T] \end{aligned} \tag{10}$$

where $\mathbf{P}(\mathbf{X},t)$ is the nominal (first Piola-Kirchhoff) stress tensor ($\mathbf{P}_{\Omega^+}$ and $\mathbf{P}_{\Omega^-}$ being its values at the domains Ω^+ and Ω^-, respectively), $\boldsymbol{\rho}_0(\mathbf{X})$ is the density $\bar{\mathbf{B}}(\mathbf{X},t)$ are the body forces, $\mathcal{T}^{\text{ ext}}(\mathbf{X},t)$ stands for the external forces applied at the boundary Γ_σ and $[0,T]$ is the time interval of interest.

As stated in Part 1, in the SDA an additional traction continuity condition should be imposed in S to induce at this interface the discrete (traction vs. displacement jump) constitutive equation. This reads:

$$\mathbf{P}_S\cdot\mathbf{N}=\mathbf{P}_{\Omega^+}\cdot\mathbf{N}\quad(=\mathbf{P}_{\Omega^-}\cdot\mathbf{N})=\mathcal{T}\qquad\text{for}\quad(\mathbf{X},t)\in S\times[0,T] \tag{11}$$

Let us consider now the following variational form at the domain Ω/S:

$$\begin{aligned} \delta\Pi_{\Omega\backslash\mathcal{S}}(\mathbf{u};\overline{\boldsymbol{\eta}})= &\int_{\Omega/\mathcal{S}}\mathbf{P}:(\overline{\boldsymbol{\eta}}\otimes\boldsymbol{\nabla}_{\mathbf{X}})\,d\Omega \\ &-\int_{\Omega/\mathcal{S}}\bar{\mathbf{B}}\cdot\overline{\boldsymbol{\eta}}d\Omega-\int_{\Gamma_\sigma}\mathcal{T}^{\text{ ext}}\cdot\overline{\boldsymbol{\eta}}\ d\Gamma=\mathbf{0} \end{aligned} \tag{12}$$

$$\forall\overline{\boldsymbol{\eta}}\ \in\bar{\mathcal{V}}_0\overset{def}{\equiv}\{\overline{\boldsymbol{\eta}}(\mathbf{X})\ ;\quad\overline{\boldsymbol{\eta}}|_{\mathbf{X}\in\Gamma_u}=\mathbf{0}\}$$

where $\bar{\mathcal{V}}_0$ is a (material) linear space of the *smooth* $\mathcal{C}^0$ functions that take null values at the prescribed displacement boundary Γ_u (admissible virtual displacements $\overline{\boldsymbol{\eta}}$). After some algebraic manipulation it can be readily shown that equations (10) are the Euler-Lagrange equations of (12). Therefore equation (12) (in fact the virtual work principle for the domain $\Omega \backslash S$) enforces, in weak form, fulfillment of the set of equations (10).

After introducing the spatial discretization of equation (4) the discrete counterpart of equation (12) reads[4]:

$$\begin{aligned} \delta\Pi^{\mathbf{h}}_{\Omega}(\mathbf{u}^{\mathbf{h}};\overline{\boldsymbol{\eta}}^h) \quad &= \int_\Omega \mathbf{P} : (\,\overline{\boldsymbol{\eta}}^h \otimes \boldsymbol{\nabla}_{\mathbf{X}})\; d\Omega - \\ &\underbrace{\int_\Omega \bar{\mathbf{B}} \cdot \overline{\boldsymbol{\eta}}^h \, d\Omega - \int_{\Gamma_\sigma} \mathcal{T}^{\text{ ext}} \cdot \overline{\boldsymbol{\eta}}^h \, d\Gamma}_{G^{ext}} = \mathbf{0} \end{aligned} \tag{13}$$

$$\forall \overline{\boldsymbol{\eta}}^h \;\in \bar{\mathcal{V}}_0^{\,h} \overset{def}{\equiv} \{\overline{\boldsymbol{\eta}}^h(\mathbf{X}) = \bar{\mathbf{N}} \cdot \boldsymbol{\delta}\mathbf{d}\;; \quad \boldsymbol{\delta}\mathbf{d}|_{\Gamma_{\mathbf{u}}} = \mathbf{0})$$

On the other hand, the nominal traction continuity condition (11) can be weakly enforced in terms of the averages of $\mathcal{T} = \mathbf{P} \cdot \mathbf{N}$ inside every element $e \in \mathcal{J}$ as follows:

$$\underbrace{\frac{1}{kl_e}\int_{S_e^k} \mathbf{P}\cdot\mathbf{N} d\Omega}_{\text{mean value of } T \text{ on } S_e^k} \quad = \quad \underbrace{\frac{1}{\Omega_e}\int_{\Omega_e} \mathbf{P}\cdot\mathbf{N}\, d\Omega}_{\text{mean value of } T \text{ on } \Omega_e}\;; \qquad \forall e \in \mathcal{J} \;\Rightarrow \tag{14}$$

$$\int_{\Omega_e} \mathbf{P}\cdot(\mu_{\mathcal{S}}^{(e)}\frac{1}{kl_e} - \frac{1}{\Omega_e})\mathbf{N}\; d\Omega = \mathbf{0} \quad ; \quad \forall e \in \mathcal{J} \tag{15}$$

where the discontinuous character of the function $\mu_{\mathcal{S}}^{(e)}$ inside the element (see equation (7)) can be captured by the integration rule sketched in figure 1e.

Finally, some algebraic manipulation of equations (13) and (15) leads to:

$$\begin{aligned} &\textstyle\int_{\Omega_i} \mathbf{P}\cdot\;(\boldsymbol{\nabla}_{\mathbf{X}}\, N_i)\;\, d\Omega \;\, - \mathbf{f}_i^{\text{ext}} = \mathbf{0} \qquad \forall i \in \{1, ..., n_{node}\} \\ &\textstyle\int_{\Omega_e} (\mu_{\mathcal{S}}^{(e)}\frac{1}{k} - \frac{l_e}{\Omega_e})\mathbf{P}\cdot\mathbf{N}\;\, d\Omega = \mathbf{0} \qquad \forall e \in \mathcal{J} \end{aligned} \tag{16}$$

[4]Observe that, due to the zero measure of the interface S and the bounded character of the integral kernels, the integration domain can be extended from $\Omega\backslash S$ to Ω.

$$\mathbf{f}_i^{\text{ext}} = \int_{\Omega_i} N_i \, \bar{\mathbf{B}} \, dV + \int_{\partial\Omega_i \cap \Gamma_\sigma} N_i \, \mathcal{T}^{\text{ext}} d\Gamma \tag{17}$$

where Ω_i stands for the support of the shape function N_i. The discrete system of equations (16) provides a set of $n_{node}+n_{\mathcal{J}}$ nonlinear equations to solve for the $n_{node}+n_{\mathcal{J}}$ unknowns $\mathbf{d} \equiv \{\mathbf{d}_1,....,\mathbf{d}_{n_{node}}\}$; $\boldsymbol{\gamma} \equiv \left\{ [[\mathbf{u}]]_1, ..., [[\mathbf{u}]]_{n_{\mathcal{J}}} \right\}$ of the discrete problem as pointed out in equation (4).

For computational purposes, and since the constitutive equations in Part 1 are given in terms of the symmetric Kirchhoff stresses $\boldsymbol{\tau} = \mathbf{P} \cdot \mathbf{F}^T$ where $\mathbf{F} = \frac{\partial \mathbf{x}}{\partial \mathbf{X}}$ is the deformation gradient tensor and $\mathbf{x}(\mathbf{X}, \mathbf{t})$ are the spatial coordinates, equation (16) can be appropriately rewritten, taking into account the identity $\boldsymbol{\nabla}_{\mathbf{X}}(\bullet) = \boldsymbol{\nabla}_{\mathbf{x}}(\bullet) \cdot \mathbf{F}$, as:

$$\boxed{\begin{array}{llll} \int_{\Omega_i} \boldsymbol{\tau} \cdot (\boldsymbol{\nabla}_{\mathbf{x}} N_i) \, d\Omega & -\mathbf{f}_i^{\text{ext}} & = \mathbf{0} \ ; & \forall i \in \{1, ..., n_{node}\} \\ \int_{\Omega_e} (\mu_{\mathcal{S}}^{(e)} \frac{1}{k} - \frac{l_e}{\Omega_e}) \ \boldsymbol{\tau} \cdot \mathbf{n} \, d\Omega & & = \mathbf{0} \ ; & \forall e \in \mathcal{J} \end{array}} \tag{18}$$

where $\mathbf{n} = \mathbf{F}^{-T} \cdot \mathbf{N}$ is the convected normal at the spatial configuration, as described in Part 1, and $(\bullet)^T$ stands for the transpose of $(\bullet)$. For the considered 2D case in a cartesian (x, y) coordinate system, equation (18) can then be cast into the classical *B-matrix* format [22] as:

$$\bigcup_{e=1}^{e=n_{elem}} \left[\int_{\Omega_e} \mathbf{B}^{(e)^T} \cdot \{\boldsymbol{\tau}\} \quad d\Omega - \mathbf{F}^{ext(e)} \right] = \mathbf{0} \tag{19}$$

where $\bigcup$ stands for the assembling operator and the elemental B-matrix, $\mathbf{B}^{(e)}$, the 2D Kirchhoff stress vector $\{\boldsymbol{\tau}\}$, and nodal forces vector, $\mathbf{F}^{\text{ext}(e)}$, are given by:

$$\boxed{\mathbf{B}^{(e)} = \left[\begin{array}{cccc} \mathbf{B}_1^{(e)} & \mathbf{B}_2^{(e)} & \mathbf{B}_3^{(e)} & \mathbf{G}^{(e)} \end{array} \right]} \tag{20}$$

$$\mathbf{B}_i^{(e)} = \begin{bmatrix} \partial_x N_i^{(e)} & 0 \\ 0 & \partial_y N_i^{(e)} \\ \partial_y N_i^{(e)} & \partial_x N_i^{(e)} \end{bmatrix} \; ; \qquad \mathbf{G}^{(e)} = (\mu_{\mathcal{S}}^{(e)} \tfrac{1}{k} - \tfrac{l_e}{\Omega_e}) \begin{bmatrix} n_x & 0 \\ 0 & n_y \\ n_y & n_x \end{bmatrix}$$

$$\{\boldsymbol{\tau}\} = \begin{bmatrix} \tau_{xx} \\ \tau_{yy} \\ \tau_{xy} \end{bmatrix} \; ; \quad \mathbf{n} = \begin{bmatrix} n_x \\ n_x \end{bmatrix} \; ; \quad \mathbf{F}^{ext(e)} = \begin{bmatrix} \mathbf{f}_1^{\mathrm{ext}(e)} \\ \mathbf{f}_2^{\mathrm{ext}(e)} \\ \mathbf{f}_3^{\mathrm{ext}(e)} \\ \mathbf{0} \end{bmatrix} \tag{21}$$

The structure of equations (20) and (21) suggests the introduction of an internal additional fourth node for each element e, that is activated only for the elements crossed by the discontinuity interface ($e \in \mathcal{J}$) and whose corresponding degrees of freedom and associated shape function are, respectively, the displacement jumps $[[\mathbf{u}]]_e$ and $\mathcal{M}_{\mathcal{S}}^{(e)}$ in equations (2) and (3). Since the support of $\mathcal{M}_{\mathcal{S}}^{(e)}$ is only Ω_e, those internal degrees of freedom can be eventually condensed at the elemental level and removed from the global system of equations.

2.3 Time integration and linearization

In the context of a time advancing process, the rate equation (8), within the element (e), is integrated at time $t + \Delta t$, in terms of the corresponding values at time t and the incremental values of the nodal unknowns $\Delta \mathbf{d}_i$ and $\Delta [[\mathbf{u}]]_e$, as follows[5]:

[5] As a technical detail in equation (22) notice that the elemental bandwidth is updated with one time step delay ($h_{e_{t+\Delta t}} \equiv h_e(t)$). In the context of the variable bandwidth method at the weak discontinuity regime, this explicit updating makes linear that equation, with a considerable simplification of the whole procedure while keeping the consistency of the integration method.

$$\begin{aligned}\mathbf{F}(\mathbf{X},t+\Delta t) &\overset{not}{=} \mathbf{F}_{t+\Delta t} = \\ &= \mathbf{F}_t + \Sigma_{i=1}^{i=3}\ \left[\Delta\mathbf{d}_i \otimes \nabla_{\mathbf{X}} N_i^{(e)}\right] \\ &- (\Delta[[\mathbf{u}]]_e \otimes \nabla_{\mathbf{X}} N_{sol}^{(e)} + \mu_{\mathcal{S}}^{(e)} \tfrac{1}{h_e(t)} (\Delta[[\mathbf{u}]]_e \otimes \mathbf{N}) \end{aligned} \tag{22}$$

$$\begin{cases} \Delta\mathbf{d}_i = \mathbf{d}_i(t+\Delta t) - \mathbf{d}_i(t) \\ \Delta\left[[\mathbf{u}]\right]_e = [[\mathbf{u}]]_e(t+\Delta t) - [[\mathbf{u}]]_e(t) \end{cases}$$

On the other hand, the algorithm of the continuum constitutive model updates the stresses $\boldsymbol{\tau}_{\,t+\Delta t}$ in terms of the updated gradient of deformation tensor $\mathbf{F}_{t+\Delta t}$ and the previous values of the stresses $\boldsymbol{\tau}_{\,t}$ and the internal variables q_t, and also provides the algorithmic constitutive operator $\mathcal{C}^{\text{algor}}_{t+\Delta t}$ (see Part1, Appendices I and II, for details [15]):

$$\boldsymbol{\tau}_{\,t+\Delta t} = \mathcal{F}\left(\mathbf{F}_{t+\Delta t}, \boldsymbol{\tau}_{\,t}, q_t\right) ; \quad \bar{L}_{\bar{v}}\boldsymbol{\tau}_{\,t+\Delta t} = \mathcal{C}^{\text{algor}}_{t+\Delta t} : (\boldsymbol{\nabla}_{\mathbf{x}} \otimes \dot{\mathbf{u}}_{t+\Delta t})^S \tag{23}$$

Using standard procedures [19], linearization, in the direction $\dot{\mathbf{u}}_{t+\Delta t}$, of the equilibrium equations (13) and (15) at time $t+\Delta t$ and yields:

$$\begin{aligned} &\int_{\Omega_i} (\overline{\boldsymbol{\eta}}^h \otimes \boldsymbol{\nabla}_{\mathbf{x}}) : \left[(\dot{\mathbf{u}}_{t+\Delta t} \otimes \boldsymbol{\nabla}_{\mathbf{x}}) \cdot \boldsymbol{\tau}_{\,t+\Delta t} + \bar{L}_{\bar{v}}(\boldsymbol{\tau}_{t+\Delta t})\right] d\Omega \ - \dot{G}^{ext} = \mathbf{0} \\ &\int_{\Omega_e} \left(\mu_{\mathcal{S}}^{(e)} \tfrac{1}{k} - \tfrac{l_e}{\Omega_e}\right) \left[(\dot{\mathbf{u}}_{t+\Delta t} \otimes \boldsymbol{\nabla}_{\mathbf{x}}) \cdot \boldsymbol{\tau}_{\mathbf{t}+\Delta\mathbf{t}} \cdot \mathbf{n} + \bar{L}_{\bar{v}}(\boldsymbol{\tau}_{t+\Delta t}) \cdot \mathbf{n}\right] d\Omega = 0 \\ &\qquad \forall \overline{\boldsymbol{\eta}}^h \in \bar{\mathcal{V}}_{\,0}^{\,h} ; \qquad \forall e \in \mathcal{J} \end{aligned} \tag{24}$$

which, after substitution of equation (23) ($\bar{L}_{\bar{v}}\boldsymbol{\tau}_{\,t+\Delta t} = \mathcal{C}^{\text{algor}}_{t+\Delta t} : (\boldsymbol{\nabla}_{\mathbf{x}} \otimes \dot{\mathbf{u}}_{t+\Delta t})^S$) and some algebraic manipulation, reads:

$$\begin{aligned} &\int_{\Omega_i} (\overline{\boldsymbol{\eta}}^h \otimes \boldsymbol{\nabla}_{\mathbf{x}}) : \left[(\mathbf{1} \bar{\otimes} \boldsymbol{\tau}_{\,t+\Delta t}) + \mathcal{C}^{\text{algor}}_{t+\Delta t}\right] : (\boldsymbol{\nabla}_{\mathbf{x}} \otimes \dot{\mathbf{u}}_{t+\Delta t}) \ d\Omega - \dot{G}^{ext} = \mathbf{0} \\ &\int_{\Omega_e} \left(\mu_{\mathcal{S}}^{(e)} \tfrac{1}{k} m - \tfrac{l_e}{\Omega_e}\right) \mathbf{n} \cdot \left[(\boldsymbol{\tau}_{\,t+\Delta t} \otimes \mathbf{1}) + \mathcal{C}^{\text{algor}}_{t+\Delta t}\right] : (\boldsymbol{\nabla}_{\mathbf{x}} \otimes \dot{\mathbf{u}}_{t+\Delta t}) \ d\Omega = 0 \\ &\qquad \forall \overline{\boldsymbol{\eta}}^h \in \bar{\mathcal{V}}_{\,0}^{\,h} ; \qquad \forall e \in \mathcal{J} \end{aligned} \tag{25}$$

were $(\mathbf{1}\bar{\otimes}\boldsymbol{\tau}_{t+\Delta t})_{ijkl} \stackrel{def}{=} \delta_{ik}\tau_{jl}$ and $(\boldsymbol{\tau}_{t+\Delta t}\otimes\mathbf{1})_{ijkl} = \tau_{il}\delta_{jk}$. From equations (2), (3) and (13), the terms $\boldsymbol{\nabla}_{\mathbf{x}}\otimes\dot{\mathbf{u}}_{t+\Delta t}$ and $(\overline{\boldsymbol{\eta}}^{h}\otimes\boldsymbol{\nabla}_{\mathbf{x}})$ in equation (24) can be expressed in discrete form as:

$$\begin{aligned}\boldsymbol{\nabla}_{\mathbf{x}}\otimes\dot{\mathbf{u}}_{t+\Delta t} = \;& \Sigma_{i=1}^{i=3}\nabla_{\mathbf{x}}N_i^{(e)}\otimes\dot{\mathbf{d}}_{i_{t+\Delta t}} + \mu_{\mathcal{S}}^{(e)}\tfrac{1}{h_e(t)}\mathbf{n}\otimes[[\dot{\mathbf{u}}]]_{e_{t+\Delta t}} \\ & -\nabla_{\mathbf{x}}N_{sol}^{(e)}\otimes[[\dot{\mathbf{u}}]]_{e_{t+\Delta t}} \\ & \overline{\boldsymbol{\eta}}^{h}\otimes\boldsymbol{\nabla}_{\mathbf{x}} = \Sigma_{i=1}^{i=3}\delta\mathbf{d}\otimes\nabla_{\mathbf{x}}N_i^{(e)}\end{aligned} \tag{26}$$

After insertion of equation (26) and some algebraic manipulations equation (25) can be rewritten, in discrete form and for the 2D problem in a cartesian (x, y) coordinate system, in the following *B-matrix* format:

$$\begin{aligned}\bigcup_{e=1}^{e=n_{elem}} & \underbrace{\left[\int_{\Omega_e}\mathbf{B}_{geo}^{(e)^T}\cdot[\hat{\boldsymbol{\tau}}_{t+\Delta t}]\cdot\mathbf{B}_{geo}^{*(e)}d\Omega\right.}_{K_{geo}} + \underbrace{\left.\int_{\Omega_e}\mathbf{B}^{(e)^T}\cdot\mathbf{c}_{t+\Delta t}^{a\,\mathrm{lg}}\cdot\mathbf{B}^{*(e)}d\Omega\right]}_{K_{mat}} \\ & \cdot\begin{bmatrix}\dot{\mathbf{d}}^{(e)}\\ [[\dot{\mathbf{u}}]]_e\end{bmatrix}_{t+\Delta t} = \dot{\mathbf{F}}_{t+\Delta t}^{ext(e)}\end{aligned} \tag{27}$$

where $\mathbf{F}^{ext\;e}$ is given in equation (21) and $\mathbf{K}_{geo}$ and $\mathbf{K}_{mat}$ can be recognized, respectively, as the classical *geometrical* and *material* tangent stiffness [22]. The remaining terms of equation (27) can be described as:

$$
\begin{aligned}
&\mathbf{B}^{(e)}=\left[\begin{array}{cccc}\mathbf{B}_1^{(e)}, & \mathbf{B}_2^{(e)}, & \mathbf{B}_3^{(e)}, & \mathbf{G}^{(e)}\end{array}\right]\\
&\mathbf{B}^{*(e)}=\left[\begin{array}{cccc}\mathbf{B}_1^{(e)}, & \mathbf{B}_2^{(e)}, & \mathbf{B}_3^{(e)}, & \mathbf{G}_{t+\Delta t}^{*(e)}\end{array}\right]\\
&\mathbf{B}_i^{(e)}=\left[\begin{array}{cc}\partial_x N_i^{(e)} & 0\\ 0 & \partial_y N_i^{(e)}\\ \partial_y N_i^{(e)} & \partial_x N_i^{(e)}\end{array}\right]\ ;\ \mathbf{G}^{(e)}=(\mu_{\mathcal{S}}^{(e)}\tfrac{1}{k}-\tfrac{l_e}{\Omega_e})\left[\begin{array}{cc}n_x & 0\\ 0 & n_y\\ n_y & n_x\end{array}\right]\\
&\mathbf{G}_{t+\Delta t}^{*(e)}=\mu_{\mathcal{S}}^{(e)}\tfrac{1}{h_e(t)}\left[\begin{array}{cc}n_x & 0\\ 0 & n_y\\ n_y & n_x\end{array}\right]-\left[\begin{array}{cc}\partial_x N_{sol}^{(e)} & 0\\ 0 & \partial_y N_{sol}^{(e)}\\ \partial_y N_{sol}^{(e)} & \partial_x N_{sol}^{(e)}\end{array}\right]
\end{aligned}
\tag{28}
$$

$$
\begin{aligned}
&\mathbf{B}_{geo}^{(e)}=\left[\begin{array}{cccc}\mathbf{B}_{geo_1}^{(e)}, & \mathbf{B}_{geo_2}^{(e)}, & \mathbf{B}_{geo_3}^{(e)}, & \mathbf{G}_{geo}^{(e)}\end{array}\right]\\
&\mathbf{B}_{geo}^{*(e)}=\left[\begin{array}{cccc}\mathbf{B}_{geo_1}^{(e)}, & \mathbf{B}_{geo_2}^{(e)}, & \mathbf{B}_{geo_3}^{(e)}, & \mathbf{G}_{geo_{t+\Delta t}}^{*(e)}\end{array}\right]\\
&\mathbf{B}_{geo_i}^{(e)}=\left[\begin{array}{cc}\partial_x N_i^{(e)} & 0\\ \partial_y N_i^{(e)} & 0\\ 0 & \partial_x N_i^{(e)}\\ 0 & \partial_y N_i^{(e)}\end{array}\right]\ ;\ \mathbf{G}_{geo}^{(e)}=(\mu_{\mathcal{S}}^{(e)}\tfrac{1}{k}-\tfrac{l_e}{\Omega_e})\left[\begin{array}{cc}n_x^{(e)} & 0\\ n_y^{(e)} & 0\\ 0 & n_x^{(e)}\\ 0 & n_y^{(e)}\end{array}\right]\\
&\mathbf{G}_{geo_{t+\Delta t}}^{*(e)}=\mu_{\mathcal{S}}^{(e)}\tfrac{1}{h_e(t)}\left[\begin{array}{cc}n_x^{(e)} & 0\\ n_y^{(e)} & 0\\ 0 & n_x^{(e)}\\ 0 & n_y^{(e)}\end{array}\right]-\left[\begin{array}{cc}\partial_x N_{sol}^{(e)} & 0\\ \partial_y N_{sol}^{(e)} & 0\\ 0 & \partial_x N_{sol}^{(e)}\\ 0 & \partial_y N_{sol}^{(e)}\end{array}\right]
\end{aligned}
\tag{29}
$$

$$\widehat{\boldsymbol{\tau}} = \begin{bmatrix} \tau_{xx} & \tau_{xy} & 0 & 0 \\ \tau_{xy} & \tau_{yy} & 0 & 0 \\ 0 & 0 & \tau_{xx} & \tau_{xy} \\ 0 & 0 & \tau_{xy} & \tau_{yy} \end{bmatrix}$$

$$\left\{ \bar{L}_{\bar{v}} \boldsymbol{\tau} \right\} = \begin{bmatrix} (\bar{L}_{\bar{v}} \tau)_{xx} \\ (\bar{L}_{\bar{v}} \tau)_{yy} \\ (\bar{L}_{\bar{v}} \tau)_{xy} \end{bmatrix} \; ; \quad \left\{ \boldsymbol{\nabla}_{\mathbf{x}} \otimes \dot{\mathbf{u}}_{t+\Delta t} \right\} = \begin{bmatrix} \partial_x \dot{u}_x \\ \partial_y \dot{u}_y \\ \partial_y \dot{u}_x + \partial_{xy} \dot{u}_y \end{bmatrix}_{t+\Delta t} \tag{30}$$

$$\begin{array}{c} \bar{L}_{\bar{v}} \boldsymbol{\tau}_{\,t+\Delta t} = \mathcal{C}^{\text{algor}}_{t+\Delta t} : (\boldsymbol{\nabla}_{\mathbf{x}} \otimes \dot{\mathbf{u}}_{t+\Delta t})^S \\ \Updownarrow \\ \left\{ \bar{L}_{\bar{v}} \boldsymbol{\tau}_{\,t+\Delta t} \right\} = \mathbf{c}^{a\,\text{lg}}_{t+\Delta t} \cdot \left\{ \boldsymbol{\nabla}_{\mathbf{x}} \otimes \dot{\mathbf{u}}_{t+\Delta t} \right\} \end{array}$$

Observe that, due to the differences $\mathbf{B}^{(e)} \neq \mathbf{B}^{*(e)}$ and $\mathbf{B}^{(e)}_{geo} \neq \mathbf{B}^{*(e)}_{geo}$ (emerging from the different matrices $\mathbf{G}^{e)} \neq \mathbf{G}^{*(e)}$ and $\mathbf{G}^{(e)}_{geo} \neq \mathbf{G}^{(e)}_{geo}$) in equations (28) and (29), the tangent stiffness $\mathbf{K} = \mathbf{K}_{geo} + \mathbf{K}_{mat}$, in equation (27), is not symmetric. This should be expected from the continuum formulation of the problem since the traction continuity equation (11) has not been imposed from the variational principle (12), but enforced in an average or *weighting* procedure through equation (14). This fact confers to the presented finite element procedure the character of a Petrov-Galerkin finite element approximation in front of the classical Galerkin-based finite element approaches. The resulting procedure has been sometimes termed, in infinitesimal strain settings, the *Statically and Kinematically Optimal Nonsymmetric* formulation [8], emphasizing its improved behavior in front of other symmetric alternative finite elements with embedded discontinuities.

3 NUMERICAL SIMULATIONS

In this section the numerical method described above are applied to the simulation of different problems where strong discontinuities develop. The main goal is to show that these numerical simulations behave as predicted by the theoretical analyzes in Part I, as well as to highlight the role of large strain kinematics in the obtained results in comparison with those obtained in infinitesimal strain settings.

The constitutive models considered in the simulations are the ones described and studied in Part I of this work [15] i.e. an isotropic continuum damage model and an elastoplastic model both considering large strains.

3.1 Damage models

3.1.1 Specimen under biaxial stress state

This example highlights the role of the variable bandwidth model described in Part1 in the SDA. A square specimen is subjected to a biaxial stress state by imposing a constant displacement u_y and a gradually increasing displacement u_x on the upper and right edges of the plate respectively, see figure 3a. As the total change in the specimen's geometry during the experiment is small[6], it can be considered that the stress σ_{yy} remains constant.

The material is characterized by the following parameters: elastic Lame's parameters $\lambda = 0.[MPa]$, $\mu = E/2 = 1.10^4[MPa]$, continuum softening parameter $\mathcal{H} = -0.125[MPa]$, discrete softening parameter $\bar{\mathcal{H}} = -0.125[MPa \cdot cm^{-1}]$,

The damage criterion is that defined in Appendix I of Part 1, with $\mu_\phi = \mu$ and $\lambda_\phi = \lambda$. Under these circumstances the elastic threshold results $r_0 = q_0 = \sigma_u/\sqrt{E} = 0.00707[MPa]^{1/2}$ (where $\sigma_u = 1.[MPa]$ stands for the uniaxial strength and E =$2.10^4[MPa]$ for the Young modulus).

The bifurcation analysis determines the normal to the discontinuity interface as $\mathbf{e}_n = (1, 0)^T$ and the only nontrivial strong discontinuity condition is $\sigma_{xx}\sigma_{yy} - \sigma_{xy}^2 = 0$. Since, due to the geometrical symmetries and loading conditions, $\sigma_{xy} = 0$, the strong discontinuity condition reads $\sigma_{yy} = 0$ which clearly is not trivially fulfilled at the bifurcation time t_B. Therefore bifurcation takes place under the form of a weak discontinuity, and a weak-strong discontinuity transition regime has to be introduced. This is governed by a variable bandwidth law $h(q)$, given by (see figure 3b):

[6]Even though the changes in the specimen geometry are small and, therefore, the behaviour at the bulk of the specimen is supposed to be the same than in infinitesimal strain settings, the large strain kinematics applied to the discontinuous interface will provide different results than in the small strains case.

$$
\begin{array}{lll}
h = h_0 = 1 \; ; & t \leq t_B & (q > q_B) \\
h = k + \frac{h_0 - k}{q_B - q_{SD}} \, q \; ; & t_B < t < t_{SD} & (q_{SD} < q < q_B) \\
h = k \; ; & t > t_{SD} & (q < q_{SD})
\end{array} \tag{31}
$$

where q_B and with q_{SD} stand for the values of the internal variable q at the bifurcation time, t_B, and at the strong discontinuity time, t_{SD}, respectively. The value q_{SD} is defined as $q_{SD} = (1 - \gamma) q_B$ ($\gamma \in [0, 1]$). Therefore, the transition factor γ determines the size of the weak discontinuity interval $[q_{SD}, q_B]$ so that for $\gamma = 0$ there is no weak discontinuity regime ($q_{SD} = q_B$) and the bifurcation is imposed under a form of a strong discontinuity. On the other hand, if $\gamma = 1$ then $q_{SD} = 0$ and all the post-bifurcation stage will be traced as a weak discontinuity.

As a matter of example, results, obtained with several values of γ, are presented in figurer 3c and 3d.

- For a very short transition regime[7], determined by a small transition factor $\gamma = 0.05$, it appears an unexpected reloading (in terms of $P_x - u_x$ response) immediately after bifurcation (see point A in figure 3c) followed by the regular expected unloading response. This can be explained as follows: since after bifurcation an incrementally elastic behavior is algorithmically imposed at $\Omega \backslash S$, as expected from the theoretical bifurcation analysis in Part 1, violation of the strong discontinuity conditions make the stresses at that point infringe the damage criterion as the process evolution proceeds (see figure 3e). This results in an artificial elastic loading at that part of the body[8] responsible, in turn, for the behavior observed in figure 3c up to point A, where the strong discontinuity condition $\sigma_{yy} = 0$ is fulfilled at S (see figure 3d). Beyond that point the strong discontinuity regime takes place and regular elastic unloading occurs at $\Omega \backslash S$ (see figure 3e) resulting in the $P_x - u_x$ unloading branch in figure 3c

- For longer (slower) transitions, determined for instance by $\gamma = 0.2$ or $\gamma = 0.5$, this *artificial reloading* is no longer observed and the transition from bifurcation to the strong discontinuity regime takes place

[7] For practical purposes this is equivalent to enforce bifurcation into a strong discontinuity.

[8] As a matter of fact if this elastic reloading takes place a "two material" constitutive equation (elastic at $\Omega \backslash S$ and elasto plastic at S) is artificially imposed by the algorithm.

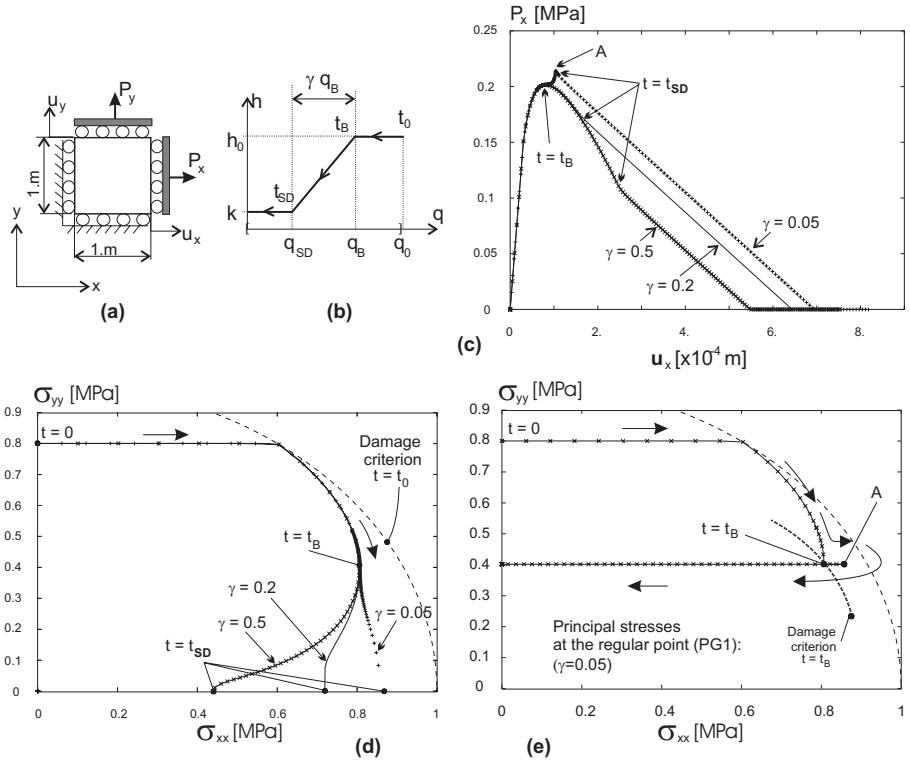

Figure 3: Square specimen: **a)** geometry and boundary conditions; **b)** bandwidth variation law h vs. q; **c)** total load P_x vs. lateral displacement u_x; **d)** equilibrium path in the principal stress plane for a point in $\mathcal{S}$ (singular Gauss point PG2 in Figure 1e; **e)** idem for a point in $\Omega/\mathcal{S}$ (regular Gauss point PG1 in Figure 1e)

smoothly as shown in figure 3c and keeping the theoretical elastic unloading at $\Omega \backslash S$.

These results confirm that, as predicted by the theoretical analyzes in Part1, the strong discontinuity kinematics can not be imposed immediately (or very shortly) after bifurcation, but a certain transition regime (weak discontinuity) is necessary to smoothly induce the strong discontinuity conditions.

In addition, it can be observed in figure 3c that the final slopes of the $P_x - u_x$ curves are the same in all cases. This could have been expected from the

fact that this part of the structural response is ruled by the induced discrete (traction-displacement jump) constitutive equation which, as it comes out from Part1, is independent of the size of the transition regime.

3.1.2 Debounding problem: Crack propagation in Mode I

This example is devoted to get some insight on the influence, on the structural response provided by the SDA, of the chosen kinematics (large or infinitesimal strain kinematics) when the regular bulk deformation (at $\Omega \backslash S$) is not small. In other words, to determine if consideration of large strains at $\Omega \backslash S$ makes any difference regardless the induced separation law at the discontinuous interface S.

For that purposes use is made of the damage model described in Part 1 [15] and its particularization to the infinitesimal strains settings given in [13].

Since the induced discrete constitutive models for both cases (infinitesimal and large strains) are different, they are made *equivalent* in terms of the fracture energy as a material property. The fracture energy G_f, defined as the external mechanical energy required per unit of surface of the discontinuity interface $\mathcal{S}$ to produce the total decohesion of the material [3], can be then computed as:

$$G_f = \int_{t_{SD}}^{t_\infty} \mathcal{T}\left(\mathbf{X}, \mathbf{t}\right) \cdot [[\dot{\mathbf{u}}]](\mathbf{X}, \mathbf{t})\, dt \tag{32}$$

where it is assumed that complete decohesion ($\mathcal{T} = \mathbf{0}$) is achieved at time t_∞.

Considering the same reference problem (uniaxial stress process) G_f can be computed and equated for both cases leading to:

$$\begin{array}{ll} \text{Small strains} & G_f = -\sigma_u^2/(2E\,\bar{\mathcal{H}}^{\text{small}}) \\ \text{Large strains} & G_f = -\sigma_u^2/(E\,\bar{\mathcal{H}}^{\text{large}}) \end{array} \Rightarrow \boxed{\bar{\mathcal{H}}^{\text{large}} = 2\bar{\mathcal{H}}^{\text{small}}} \tag{33}$$

where σ_u stands for the uniaxial peak stress and E for the Young modulus. The relationship between the discrete softening parameters $\bar{\mathcal{H}}$, obtained in equation (33), is then extended to more general stress states as an approximate way to keep the fracture energy as a common material property for large and small strain kinematics.

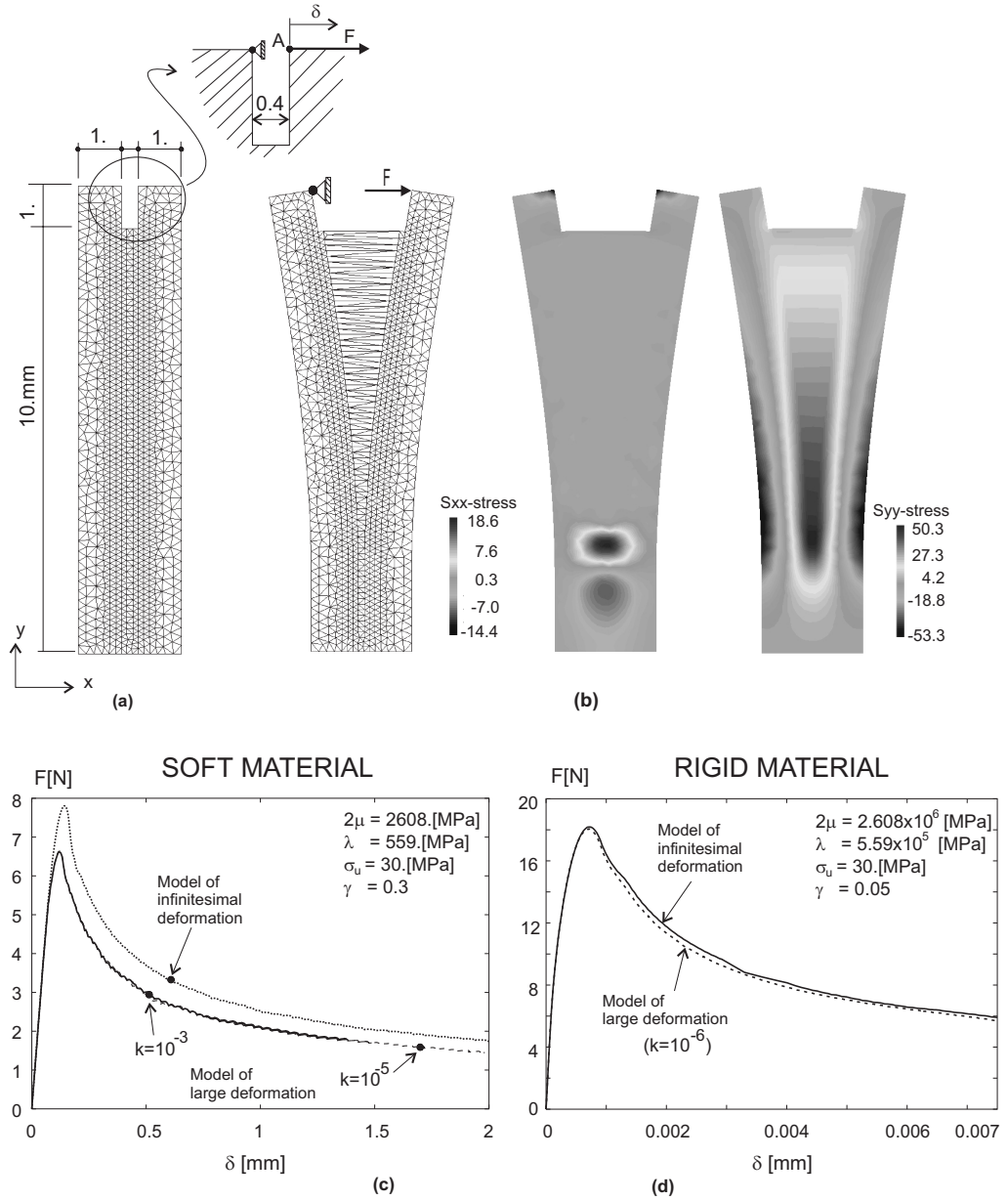

Figure 4: Crack propagation in Mode I: **a)** geometry, boundary conditions and finite element mesh; **b)** contours at the final time with the large deformation model: (deformed shape at true scale), Contours of the Cauchy stress σ_{xx} and σ_{yy}; **c)** load-displacement curves of point A with a soft material; **d)** load-displacement curves of point A with a rigid material.

With these considerations in mind, in figure 4 the simulation of a debounding process in a composite panel is presented.

Two plates, initially bound together, are enforced to separate by pulling the upper notch, as depicted in figure 4a. Both the plates and the binding material are assumed to have the same material properties, and, as a result of the loading process, a crack propagates vertically beneath the notch and along the binding.

Two different fictitious materials, both having the same G_f ($\bar{\mathcal{H}}^{\mathrm{large}} = 0.4$ and $\bar{\mathcal{H}}^{\mathrm{small}} = 0.2$) , and different elastic properties (see figures 4c and 4d) have been then considered. The rigid material has elastic properties 1000 times larger than the soft one. This precludes large elastic strains and displacements to develop at the bulk for this material, unlike the soft material case . As it can be checked in figure 4c, the results obtained assuming finite strain or infinitesimal strain kinematics are quite different for the soft material (which allows the plates to undergo large strains and displacements). However for the rigid material case, figure 4d shows very similar responses for both types of kinematics since large strains do not develop at the bulk and the separation law is made equivalent for both cases through equation (33). These analyzes confirm that, regardless the induced discrete constitutive equation, the considered kinematics does make a difference in the results if large strains can develop at bulk.

In figure 4c, invariance of the results with respect to the regularization parameter k is also shown through comparison of the results obtained with two different values ($k = 10^{-4}$ and $k = 10^{-5}$).

3.2 Elastoplastic models

In next examples the J2 plasticity model for large strains, presented in Part 1 [15], is considered in the context of the SDA.

In both cases, and following the reference works, the analysis begins by adopting a (almost) perfect elastoplastic material. After achieving a given level of deformation, a significant amount of softening is enforced in order to induce localization.

As for the bandwidth model, the same linear bandwidth variation law $h(q)$ of the damage model, (equation 31 and figure 3b) has been used here.

3.2.1 Localization in a homogeneous problem

This example is taken from references [1] and [5] where the analysis is made by introducing explicitly a discrete elastoplastic constitutive model at the interface, regardless the strong discontinuity conditions. A rectangular plate, shown in Figure 5a, is stretched by imposing a uniform displacement d at one side of the plate keeping the other side fixed.

The elastic material parameters, which correspond to the model of Appendix II in Part 1 and the plain strain case, are: $\hat{\lambda} = 110.7GPa$, $\mu = 80.2GPa$ and $\tau_y = 450.[MPa]$. The considered hardening/softening law is given in 5c; the uniaxial peak stress is $\tau_y = 450.[MPa]$ and the initial slope of the curve $\tau_y - \alpha$ is given by a very small hardening modulus; $\mathcal{H}$ =$0.1[Gpa]$[9]. At a certain (*imposed*) value α_{bif} , of the internal variable α, the hardening/softening modulus is modified to the negative value $\mathcal{H} = -12.[Gpa]$ in order to induce an immediate bifurcation and the corresponding localization at the band of elements crossed by a (straight) discontinuity interface S[10]. Therefore, varying the value α_{bif} one can induce an early bifurcation (for small values of α_{bif}) or a late bifurcation (for large values of α_{bif}).

Once again, the purpose of this simulation is to highlight the role of the strong discontinuity conditions and to show that, even though the numerical results can, sometimes, hide its role they can not be, in general, neglected.

In figure 5d the Cauchy stress (at the bulk) $\sigma_{\Omega/S}$ vs. the displacement d are plotted for two different values of α_{bif} i.e.:

1) A small value $\alpha_{bif} = 0.0025$. This corresponds, for practical purposes, to not considering any perfect plasticity branch before the bifurcation, which is induced immediately after yielding.

2) A large value $\alpha_{bif} = 0.025$. This corresponds to considering a relatively large perfect plasticity branch as made in reference [1].

As for the variable bandwidth model two different values of the transition factor γ are considered:

[9] For practical purposes this can be considered a *perfect plasticity* branch.

[10] Since the geometry and the material properties make the problem, and the pre-localization stress field, homogeneous, the position of the discontinuity interface is enforced to pass through a given point (point A in figure 5b).

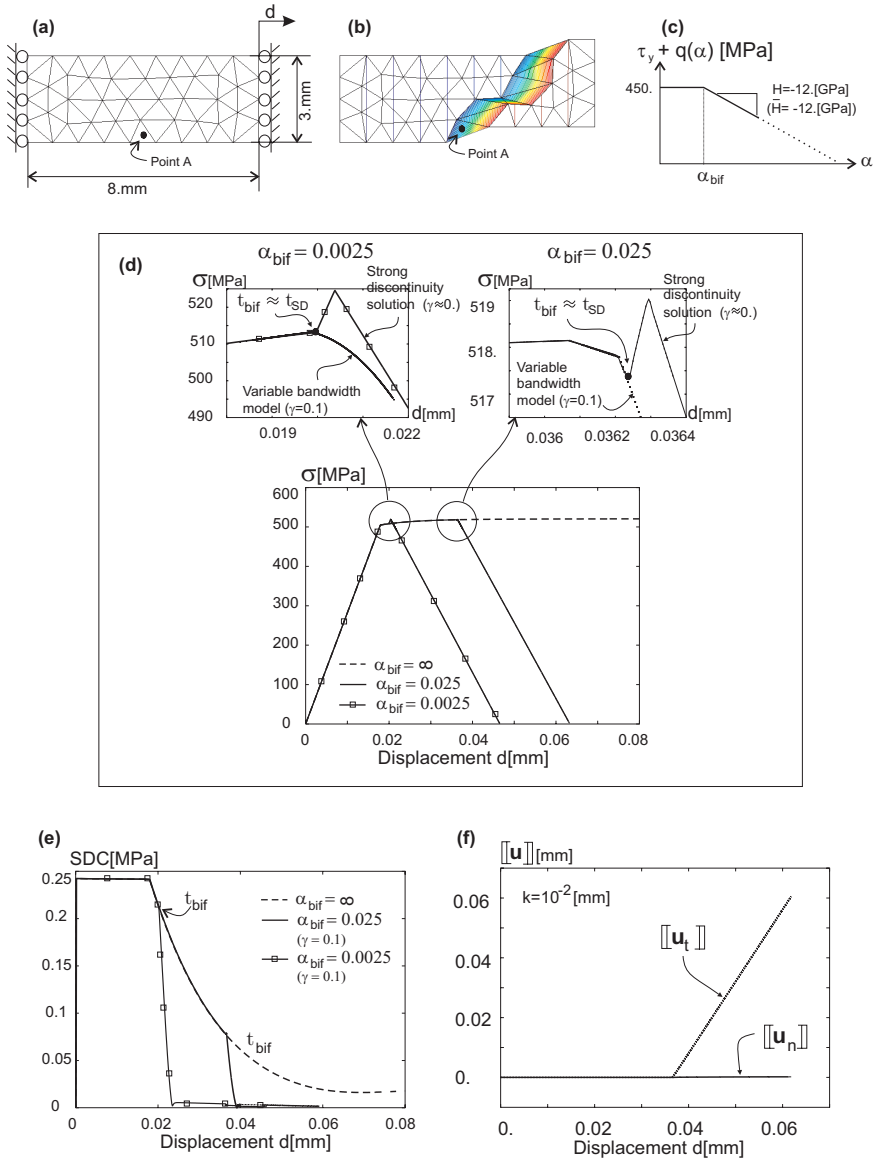

Figure 5: Localization in a homogeneous problem: **a)** geometrical model and finite element mesh; **b)** deformed mesh and contours of horizontal displacements; **c)** hardening/softening law; **d)** horizontal stress vs. edge displacement curves for different lengths of the perfect plasticity branch; **e)** evolution of the strong discontinuity conditions; **f)** normal and tangential displacement jump of point A vs. edge displacement; **g)** normal vs. tangential displacement jumps.

a) A very small transition factor $\gamma = 0.001$. For practical purposes this corresponds to an immediate imposition of a strong discontinuity kinematics after the bifurcation. In the plots the corresponding results are labelled *strong discontinuity solution* and are equivalent to impose the induced discrete constitutive equation immediately after the bifurcation as it is done in reference [1].

b) A non negligible transition factor $\gamma = 0.1$. This corresponds to introducing a *weak discontinuity regime* immediately after the bifurcation, for approximately the first 10% of the softening response, to gradually induce the strong discontinuity. In the plots the corresponding results are labelled *variable bandwidth model*.

Amplified plots of this curves around the bifurcation are also shown in the same figure 5-(d). It is remarkable the unphysical response obtained for the strong discontinuity case ($\gamma = 0.001$), since unexpected reloading takes place immediately after bifurcation, translating into sharp peaks in the curves. Although the amount of this reloading is smaller for the large perfect plasticity branch ($\alpha_{bif} = 0.025$) and it is somehow *hidden* in the global plot, the amplification shows clearly that the problem is still there *an so are the same type of inconsistencies than for the short perfect plasticity branch*. On the contrary, this problem does not show up in the results obtained with the variable bandwidth model ($\gamma = 0.1$) which are smooth with no reloading effect as can be checked in the figure.

The explanation for such phenomena can be found in the strong discontinuity conditions as in the example in section 3.1.1. The strong discontinuity conditions for the plain strain case can be written, according to the strong discontinuity analysis made in Part 1, in terms of the deviatoric components of the Kirchoff stresses $\boldsymbol{\tau}^{dev}$as:

$$\tau_{11}^{dev} = \tau_{22}^{dev} = \tau_{33}^{dev} = 0 \tag{34}$$

where a cartesian system of coordinates with the third direction orthogonal to the plane of analysis has been considered. To evaluate the degree of fulfillment of equations (34) in a scalar variable, the value $SDC = \sqrt{(\tau_{11}^{dev})^2 + (\tau_{22}^{dev})^2 + (\tau_{33}^{dev})^2}$ has been computed along the deformation process and plotted in figure 5e. It can be observed there that, for the perfect plasticity case ($\alpha_{bif} = \infty$), the value SDC tends asymptotically to zero, so that *the*

strong discontinuity conditions are never fulfilled in perfect plasticity regardless the length of the horizontal branch. This explains the reloading peaks observed in 5d as a consequence of the lack of fulfillment of the strong discontinuity conditions at the bifurcation combined with the immediate imposition of a strong discontinuity kinematics. However, if the variable bandwidth model is considered after bifurcation, the strong discontinuity conditions are quickly, but smoothly, fulfilled at the end of the transition regime, as it can be checked in figure 5e for the transition factor $\gamma = 0.1$, this explaining the absence of the unphysical reloading peaks in 5e.

Finally, in figure 5-(f) the normal ($[[u_n]]$) and tangential ($[[u_t]]$) components of the displacement jump at point A in figure 5b are plotted. It can be checked as the displacement jump is null all along the deformation process as it was predicted by the strong discontinuity analysis of Part 1 for plasticity models in finite deformation settings. Notice that condition $[[u_n]] = 0$ is not explicitly imposed by the continuum format of the constitutive model, and its fulfillment in the numerical simulation constitutes a proof that the discrete constitutive equation predicted in the theoretical analysis is actually induced during the simulation.

3.2.2 Localized shearing in a plane strain specimen with substantial necking

This problem has been taken from reference [9] here considering a different localization mode. The goal of this simulation is to apply the SDA to a problem were considerable concentration of the strains, producing substantial necking and the corresponding large regular strains, takes place before a real bifurcation an the subsequent strong discontinuity occur.

In figure 6a the geometrical characteristics of the problem are presented. The specimen, in plain strain, is stretched by applying a uniform vertical displacement at the top edge. Due to the symmetry of the problem, only 1/4 of the structure is modelled using two different finite element meshes (Meshes A and B in figure 6c). Mesh A is not structured while Mesh B is a structured one with a particular pattern of triangles to alleviate the possible numerical locking due to the incompressibility of plastic flow, as it has been reported in the classical literature [11].

The continuum constitutive model is the J2 plasticity one described in Part 1. The elastic material parameters are: $\hat{\lambda} = 80.[GPa]$ and $\mu = 80.[GPa]$ and the hardening/softening law is given in figure 6b. The uniaxial peak

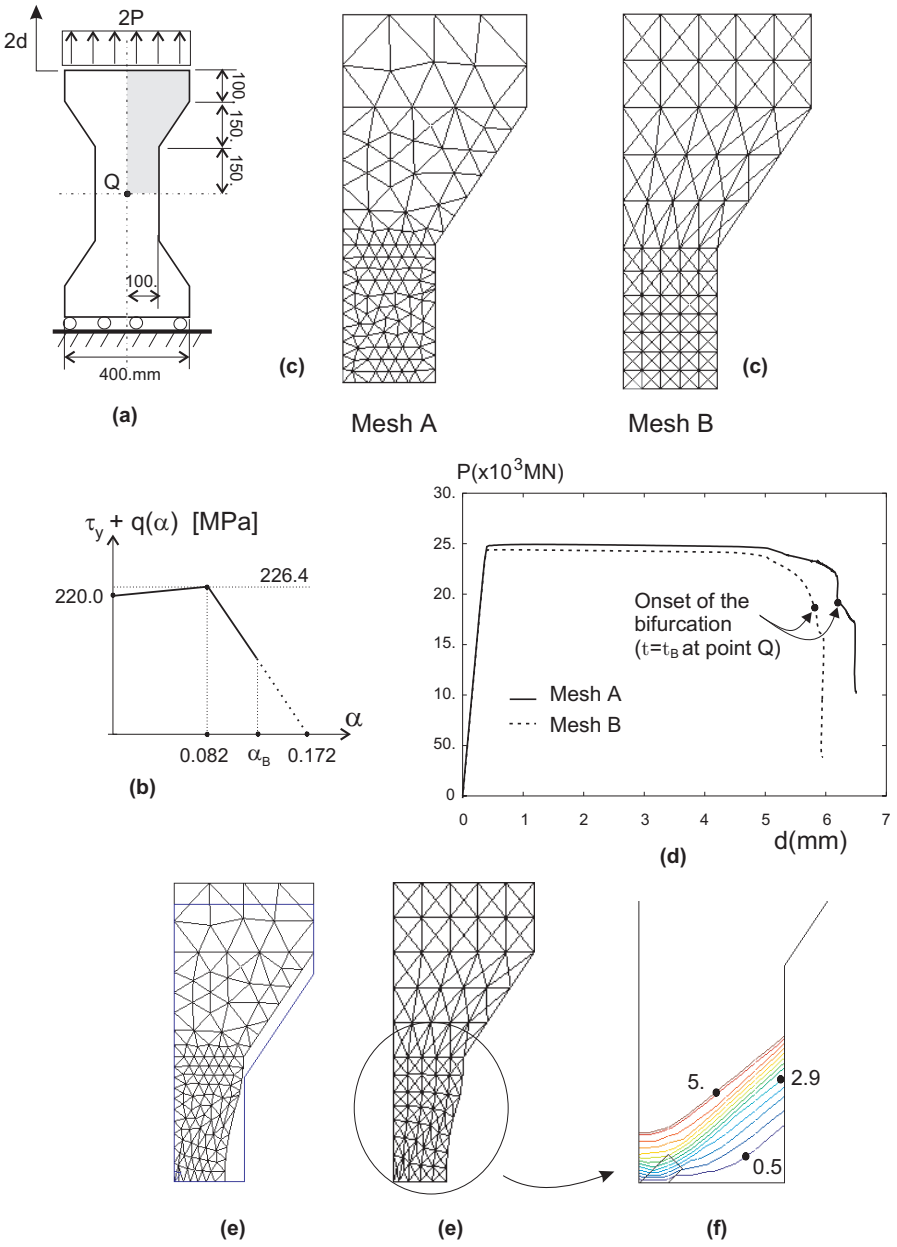

Figure 6: Localized shearing in a plane strain specimen with necking: **a)** geometrical model; **b)** softening law; **c)** finite element meshes; **d)** load vs. displacement curves; **e)** deformed meshes at final stages of the analysis; **f)** contours of vertical displacement.

stress is $\tau_y = 220.[MPa]$ and the discrete softening parameter is $\bar{H} = -2515[MPa]$. The transition factor is $\gamma = 0.4$

Figure 6d, shows the load vs. displacement curves obtained with meshes A and B. It is observed that in the first part of the curves, before the sharp softening, both of them give very similar results. The slight difference which arise before the onset of bifurcation, can be caused by locking effects in mesh A. However, in the post bifurcation regime, both meshes exhibit a similar response showing that the possible pre-bifurcation locking does not crucially affect the development of the strong discontinuity regime.

In figure 6e the final deformed meshes are presented showing a considerable amount of necking. Unlike what happens when the pre-bifurcation strains are small, the concentration of the strains in a non-zero bandwidth zone smears the displacements contours out of the band of elements crossed by the discontinuous interface S (see figure 6f). Anyway, the classically reported orientation of the localization in a band forming about 45^o with the horizontal can be clearly noticed.

4 CONCLUDING REMARKS

In this second part of the work a numerical methodology for the application of the Strong Discontinuity Approach in large strains and finite element contexts has been presented.

As for the considered family of finite elements with embedded discontinuity, it does not conceptually differ much from the one used in infinitesimal strain settings. Through the numerical simulations performed in this work, it has been proved its ability to capture strong discontinuities also when large strain kinematics are considered. The main drawback of this type of finite element, the necessity of a global[11] algorithm to track the discontinuity across the finite element mesh, remains in the large strains context. The global character of this algorithm makes its implementation in typical finite element codes cumbersome, and difficult to deal with multiple crack problems, branching phenomena etc.

The numerical simulations carried out, also corroborate the predictions of the strong discontinuity analyzes made in Part 1 i.e.:

[11] The *global character* means that the algorithm can not be implemented only affecting the *one element level* (local level) of a finite element code, but at higher levels of the algorithmic structure of the code.

- The relevance of the strong discontinuity conditions and the role of the transition (weak discontinuity) regime, and the proposed variable bandwidth model, to make the simulations physically consistent[14].

- The role of the type of kinematics (large or small strains) in the simulations results. As general conclusions it can be said that:

    1. The induced discrete constitutive equations depend, in general, on the considered kinematics. For instance using the considered damage model, as it has been shown in section 3.1.2, for uniaxial stress cases results in a factor of 2, in the value of the resulting discrete softening parameter $\bar{\mathcal{H}}$ for large/small strains, if the same value of the fracture energy G_f is considered .
    2. Even if the same large strain setting is considered, whether large or small strains are actually developed at the regular part of the body causes substantial differences in the obtained results. In the context of the SDA this fact would eventually justify the use of its large strains counterpart that has been presented in this work.

Acknowledgements

The second author acknowledges the Secretaria de Estado de Educación, de Universidades, Investigación y Desarrollo of Spain for the financial support received. The fourth author acknowledges the Agencia Española de Cooperación Internacional (AECI) for its financial support.

References

[1] F. Armero. Large-scale modelling of localized dissipative mechanism in a local continuum: applications to the numerical simulation of strain localization in rate-dependent inelastic solids. *Mech. of Cohesive-Frictional Materials*, 4:101–131, 1999.

[2] F. Armero and K. Garikipati. An analysis of strong discontinuities in multiplicative finite strain plasticity and their relation with the numerical simulation of strain localization in solids. *Int.J. Solids and Structures*, 33(20–22):2863–2885, 1996.

[3] Z.P. Bazant and J. Planas. *Fracture and size effect in concrete and other quasibrittle materials*. CRC Press, 1998.

[4] T. Belytschko, N. Moes, S. Usui, and C. Parimi. Arbitrary discontinuities in finite elements. *Int. J. Numer. Meth. Engng.*, (50):993–1013, 2001.

[5] C.C.Celigoj. On strong discontinuities in anelastic solids. A finite element approach taking a frame indifferent gradient of the discontinuous displacements. *Int. J. Numer. Meth. Engng.*, (49):769–796, 2000.

[6] E.N. Dvorkin, A.M. Cuitino, and G. Gioia. Finite elements with displacement embedded localization lines insensitive to mesh size and distortions. *International journal for numerical methods in engineering*, 30:541–564, 1990.

[7] K. Garikipati and T.J.R. Hughes. A variational multiscale approach to strain localization for multidimensional problems. *Comput. Methods Appl. Mech. Engrg.*, (188):39–60, 2000.

[8] M. Jirasek. Comparative study on finite elements with embedded discontinuities. *Comput. Methods Appl. Mech. Engrg.*, (188):307–330, 2000.

[9] R. Larsson, P. Steinmann, and K. Runesson. Finite element embedded localization band for finite strain plasticity based on a regularized strong discontinuity. *Mechanics of Cohesive Frictional Materials*, 4:171–194, 1998.

[10] H.R. Lofti and P.Benson Ching. Embedded representation of fracture in concrete with mixed finite elements. *International journal for numerical methods in engineering*, 38:1307–1325, 1995.

[11] A. Needleman and V. Tvergaar. *Finite element analyisis of localization in plasticity. In: Finite Elements, Special Problems in Solid Mechanics*, volume V, pages 94–157. Prentice-Hall, Englewood Cliffs, 1984.

[12] J. Oliver. Modeling strong discontinuities in solid mechanics via strain softening constitutive equations. Part 2: Numerical simulation. *Int.J.Num.Meth.Eng.*, 39(21):3601–3623, 1996.

[13] J. Oliver. On the discrete constitutive models induced by strong discontinuity kinematics and continuum constitutive equations. *International Journal Solids and Structures*, 37:7207–7229, 2000.

[14] J. Oliver, A. Huespe, M.D.G. Pulido, and E. Chaves. From continuum mechanics to fracture mechanics: the strong discontinuity approach. *Engineering Fracture Mechanics*, (in press), 2001.

[15] J. Oliver, A.E. Huespe, M.D.G. Pulido, and E. Samaniego. On the strong discontinuity approach in finite deformation settings. part 1: Theoretical aspects. *Submitted to Int. J. Numer. Meth. Engng.*

[16] N.S. Ottosen and K. Runesson. Properties of discontinuous bifurcation solutions in elasto-plasticity. *Int. J. Solids and Structures*, 27(4):401–421, 1991.

[17] R.A. Regueiro and R. I. Borja. Plane strain finite element analysis of presure sensitive plasticity with strong discontinuity. *International Journal of Solids and Structures*, (38):3647–3672, 2001.

[18] J. Simo and J. Oliver. A new approach to the analysis and simulation of strong discontinuities. In Z.P. Bazant et al., editor, *Fracture and Damage in Quasi-brittle Structures*, pages 25–39, 1994. E & FN Spon.

[19] J.C. Simo and T.J.R. Hughes. *Computational Inelasticity*. Springer, 1998.

[20] G.N. Wells and L.J. Sluys. A new method for modelling cohesive cracks using finite elements. *Int. J. Numer. Meth. Engng*, (50):2667–2682, 2001.

[21] K. Willam. *Constitutive models for materials, in: Encyclopedia of Physical Science & Technology , 3rd edition*. Academic Press, 2000.

[22] O.C. Zienkiewicz and R.L. Taylor. *The Finite Element Method*. McGraw-Hill, London, 1989.